

Manuscript Number:

Title: Repeated Magmatic Build-up and Deep "Hot Zones" in Continental  
Evolution: the Cadomian Crust of Iran

Article Type: Letters

Keywords: Continental Crust, Magmatic Flare-up, Hot Zone, Cadomian, Iran

Corresponding Author: Dr. Hadi Shafaii Moghadam,

Corresponding Author's Institution: ARC Centre of Excellence for Core to  
Crust Fluid Systems and GEMOC ARC National Key Centre

First Author: Hadi Shafaii Moghadam

Order of Authors: Hadi Shafaii Moghadam; Qiu-li Li; William L Griffin;  
Robert J. Stern; Osamu Ishizuka; Hadrien Henry; Federico Lucci; Suzanne  
Y O'Reilly; Ghasem Ghorbani

Abstract: The generation and differentiation of continental crust by arc magmatism is strongly influenced by episodes of high magmatic flux ("flare-ups"). Magmatic flare-ups encourage the development of deep crustal hot zones where magmatic differentiation and density stratification combine to form the upper felsic and lower mafic continental crust. Such processes, which are responsible for the construction of continental arc crusts, are prolonged events, which build a ~30-40 km arc crust during tens of million years (~100 Myr). New zircon U-Pb data reveal that the construction of Cadomian crust from NE Iran occurred over ~15 Myr. However, compiled zircon U-Pb ages reveal a prolonged magmatic flare-up of ~45 Myr; ~570 to 525 Ma. Basement outcrops in NE Iran expose lower -and upper crust that show how magmatic-geochemical differentiation occurred deep beneath a Cadomian continental arc in a crustal hot zone. Isotopic data for igneous rocks produced during this 45 Myr episode reveal interactions between mantle-derived melts and old continental crust. Synthesis of new and published data indicates that this type of interaction is common during periods of high magmatic fluxes. Our results indicate that differentiation of mafic melts in the lower crust during prolonged magmatic flare-ups plays a key role in building a stratified continental crust.

Suggested Reviewers: Ulf Linnemann  
ulf.linnemann@senckenberg.de

Mihai Ducea  
U AZ, USA  
ducea@email.arizona.edu

Charles Verdel  
Queensland U Technology, Australia  
charles.verdel@qut.edu.au

Jean-Pierre Burg

ETZ  
jean-pierre.burg@erdw.ethz.ch

George Bergantz  
U. Washington  
bergantz@uw.edu

Opposed Reviewers:

Research Data Related to this Submission

-----  
Title: Data for: Repeated Magmatic Build-up and Deep "Hot Zones" in  
Continental Evolution: the Cadomian Crust of Iran  
Repository: Mendeley Data  
<https://data.mendeley.com/datasets/v25z8d95tf/draft?a=2c678169-e0d5-44bd-8eea-968355e69d73>

**Repeated Magmatic Build-up and Deep “Hot Zones” in Continental Evolution: the Cadomian Crust of Iran**

**Hadi Shafaii Moghadam<sup>1,2,3\*</sup>, Q.L. Li<sup>1</sup>, W.L. Griffin<sup>2</sup>, R. J. Stern<sup>4</sup>, O. Ishizuka<sup>5</sup>, H. Henry<sup>2</sup>, F. Lucci<sup>6</sup>, S.Y. O’Reilly<sup>2</sup> and G. Ghorbani<sup>3</sup>**

<sup>1</sup>State Key Laboratory of Lithospheric Evolution, Institute of Geology and Geophysics, Chinese Academy of Sciences, Beijing 100029, China

<sup>2</sup>Arc Centre of Excellence for Core to Crust Fluid Systems and GEMOC ARC National Key Centre, Dept. of Earth and Planetary Sciences, Macquarie University, NSW 2109, Australia

<sup>3</sup>School of Earth Sciences, Damghan University, Damghan 36716-41167, Iran

<sup>4</sup>Geosciences Dept. University of Texas at Dallas, Richardson, TX 75083-0688, USA

<sup>5</sup>Institute of Geology and Geo-information, Geological Survey of Japan, Ibaraki 305-8567, Japan

<sup>6</sup>Dipartimento di Scienze, Sezione Scienze Geologiche, Università “Roma Tre”, 1-00146 Rome, Italy

\*Corresponding authors; Hadi Shafaii Moghadam, [hadishafaii@yahoo.com](mailto:hadishafaii@yahoo.com); Qiu-li Li, [liqiuli@mail.iggcas.ac.cn](mailto:liqiuli@mail.iggcas.ac.cn)

Dear editor;

I am writing you to submit our manuscript titled, “*Repeated Magmatic Build-up and Deep “Hot Zones” in Continental Evolution: the Cadomian Crust of Iran*”. This paper deals with the processes that produced and differentiated continental crust as a result of arc magmatism and high magmatic flux in Iran during Ediacaran-Early Cambrian. Because our findings can be applied for understanding how a protracted magmatic flare-up was important for building well-stratified continental crust in the extensional arcs such as Iran, we think this contribution will be of great interest to readers of “*Earth and Planetary Science Letter*”. This manuscript is an original work and is not under consideration by any other journal. We confirm that ALL material is original and ideas that are used in interpretation are cited to proper references. All authors approved the manuscript and this submission to “*Earth and Planetary Science Letter*”. Thank you for receiving our manuscript and considering it for review. We appreciate your time and look forward to your response.

Kind regards

Hadi Shafaii Moghadam/ Qiu-li Li (Corresponding authors)

**Highlights:**

- ❖ Cadomian continental arc crust of Iran was built during ~15 Myr of magmatism.
- ❖ Magmatic flare-up in Iran occurred over ~45 Myr; 570 to 525 Ma.
- ❖ Geochemical differentiation in “hot zones” built the stratified continental crust of Iran.



## 37 **Introduction**

38 Subduction-related magmatism along the active continental margins is regarded as one of the main  
39 mechanisms for the generation of magmatic pulses within the continental crust. However, the controlling  
40 factors and time-scales producing compositional diversification within most arcs remain controversial.  
41 Arc magmatism in most subduction zones is a prolonged process, which builds a ~30-40 km arc crust  
42 over tens of millions of years (~100 Myr for continental arcs *vs* ~40 Myr for oceanic ones, [Ducea et al.,](#)  
43 [2015b](#)), although recent zircon U-Pb observations on the Sierra Valle Fertile crustal section (Famatinian  
44 arc, Argentina), show that the entire arc crust (~30 km thickness) can be built by magmatic processes  
45 within ~4 Ma ([Ducea et al., 2017](#)). These short-time magmatic processes are responsible for the  
46 construction of continental crust in some modern arcs ([Jicha and Jagoutz, 2015](#)), but their role in the  
47 building of crust in ancient arcs, such as the Neoproterozoic-Early Cambrian arcs from northern  
48 Gondwana, is enigmatic. The other ambiguities we want to understand, are the mechanisms that control  
49 the lower-middle crustal diversification in ancient arcs. Both short and prolonged magmatism in most arcs  
50 is accompanied by high-magmatic fluxes (“flare-ups”) and the removal of the deep lithosphere by  
51 delamination ([Ducea et al., 2015a](#); [Ducea et al., 2015b](#)).

52 Seismic-velocity measurements suggest that the lower- and middle crust of continental arcs is  
53 composed chiefly of gabbroic and intermediate tonalitic rocks and their metamorphic equivalents  
54 ([Kitamura et al., 2003](#)). The composition and flux of mantle-derived magmas and the processes operating  
55 on these to produce lower continental crust through continental arc magmatism have been investigated  
56 experimentally ([Christensen and Mooney, 1995](#)) and by petrological and geochemical modeling ([Jagoutz,](#)  
57 [2014](#)). Magmatic differentiation occurs at intermediate crustal levels (~20-30 km deep), mostly associated  
58 with large intrusions of intermediate to felsic composition, and in lower-crustal “deep crustal hot zones”  
59 ([Annen et al., 2006](#)) and/or mafic zones ([Walker et al., 2015](#)), where differentiating mantle-derived  
60 magmas interact with pre-existing crust, in MASH (combined Mixing, Assimilation, Storage and  
61 Homogenization) zones. Lower-crustal MASH processes can also be linked to the foundering of  
62 ultramafic-mafic cumulates and residues back into the mantle.

63 Studying lower crustal arc sections is difficult, but is possible in some places, for example Kohistan  
64 and Talkeetna. The Kohistan area (NE Pakistan) exposes juvenile continental crust formed in an Early  
65 Cretaceous oceanic arc ([Jagoutz and Schmidt, 2012](#)). Further evidence for magmatic stratification beneath  
66 arc roots comes from observations of the Jurassic Talkeetna continental arc (south-central Alaska) ([Behn](#)  
67 [and Kelemen, 2006](#)), the late Paleozoic Cabo Ortegal complex (Spain) ([Tilhac et al., 2016](#)), and the  
68 Ordovician Famatina Complex of Argentina ([Ducea et al., 2017](#); [Walker et al., 2015](#)). The aim of this  
69 study is to utilize these and other insights to evaluate the role of different magmatic fluxes in forming a  
70 differentiated crust and to better understand how the continental crust of Iran formed. This crust mostly

71 formed in Late Ediacaran and Early Cambrian time during an episode known in Europe as the Cadomian  
72 orogeny. We focus on exposures around Torud in NE Iran (Fig. 1), where lower crust and complementary  
73 upper crust are exposed, providing a quasi-continuous exposure of a Cadomian continental magmatic arc.  
74 Our results indicate that magmatic differentiation occurred predominantly in the deep crust beneath this  
75 arc, during a flare-up event. Our results strongly support the idea that deep crustal “MASH zones” existed  
76 beneath such arcs, where mafic melts differentiated, and further suggest that lower-crustal foundering  
77 associated with the hot zone was incomplete. We also show that the Cadomian arc crust of Iran was  
78 entirely formed by magmatic processes within ~15 Myr, which is significantly prolonged compared with  
79 modern arcs.

80

### 81 **Geological background**

82 The Cadomian orogen of Europe, SW Asia (Iran and Anatolia) and E. North America was a Late  
83 Ediacaran to Early Cambrian peripheral accretionary margin and magmatic arc generated above a south-  
84 dipping subduction zone along northern Gondwana ([Linnemann et al., 2010](#)). Cadomian arc magmatism  
85 in Iran and Anatolia occurred in a transtensional setting above this subduction zone to build the ribbon  
86 continent “Cimmeria” which rifted off Gondwana and accreted to Eurasia in late Paleozoic time  
87 ([Moghadam et al., 2015](#)). Cadomian arc magmatism generated the continental nuclei of Iran, with a  
88 magmatic “flare-up” in latest Ediacaran time ([Moghadam et al., 2017d](#)).  
89 Significant exposures of Cadomian magmatic rocks in Iran are known from the west (Golpayegan),  
90 northwest (Khoy-Salmas, Zanjan-Takab), northeast (Torud, Taknar) and central regions (Saghand) (Fig.  
91 1A). The Cadomian basement rocks of Iran were mostly exhumed as a result of Cenozoic extension and  
92 core-complex formation ([Verdel et al., 2007](#)). Cadomian magmatic rocks in Iran and Turkey mostly form  
93 felsic plutons (granite to tonalite) along with minor dacitic to rhyolitic extrusive rocks. Intermediate to  
94 mafic intrusive rocks are less abundant and basaltic lavas are rare.

95 Cadomian crust is exposed over about 40,000 km<sup>2</sup> in NE Iran, from NE of Torud to south of Taknar  
96 (Fig. 1B). It is overlain by Jurassic and Cretaceous metasedimentary rocks. Ar-Ar and K-Ar ages on  
97 muscovite and biotite from NE Iran orthogneisses yield ages of *ca* 160 and 171 Ma, respectively  
98 ([Rahmati-Ilkhchi et al., 2010](#)), which are interpreted as the ages of metamorphism and exhumation.  
99 Recent Ar-Ar data show that the exhumation has occurred during Late Cretaceous time, due to the  
100 extensional phases which were affecting the Iranian plateau during that time ([Malekpour-Alamdari et al.,](#)  
101 [2017](#)). Cadomian exposures in NE Iran include a section of middle to upper crust, comprising gabbroic-  
102 dioritic intrusions (U-Pb zircon age ~556 Ma) grading into a thick sequence (~20 km) of granitoid  
103 intrusions (U-Pb zircon ages ~532-552 Ma) grading upward into felsic volcanic rocks (U-Pb zircon age  
104 ~550 Ma) and psammitic to volcanogenic metasediments (with detrital U-Pb zircon ages of ~549-552

105 Ma) ([Moghadam et al., 2015](#)). Felsic and mafic (amphibolite) dikes and sills yield zircon U-Pb ages of *ca*  
106 532-554 Ma ([Hosseini et al., 2015](#)). Felsic intrusions comprise I-type granites, granodiorites and tonalites;  
107 these are isotopically variable, with initial  $\epsilon_{Nd}$  of -6 to +7, zircon  $\epsilon_{Hf}$  ranging from -9.6 to +10.7 and  
108  $\delta^{18}O$  of zircon between  $\sim+5$  to  $>+9$  ‰. These isotopic data suggest the involvement of both juvenile melts  
109 and older continental crust ([Moghadam et al., 2015](#)).

110 The recently discovered arc section in the Cadomian segment of NE Iran (Torud) integrated with the  
111 neighboring crustal exposures, is one of the best quasi-continuous vertical, but tilted deep exposures of a  
112 subduction-related Cadomian continental arc crust in Iran. The upper-crustal rocks in this area are  
113 dominated by metasediments, including paragneissic rocks and metapelites, grading downward into  
114 middle crust dominated by felsic to intermediate intrusions, interlayered with metasedimentary host-  
115 rocks. Mafic rocks are also present in the middle crust but are rare. The upper-middle crustal intrusive  
116 rocks are less to highly deformed and metamorphosed to various types of gneissic rocks, dependent of  
117 their composition (e.g., granitic gneisses to dioritic gneisses). Felsic dikes (variably metamorphosed) are  
118 abundant in the middle-crustal intrusions.

119 The middle-upper crustal section changes downward into middle-lower crustal outcrops including  
120 amphibole-bearing mafic rocks – now appearing as mylonitic gabbros, meta-gabbroids and amphibolites  
121 with a cumulate-like texture; hereafter referred to as cumulate rocks – with a total thickness of  $\sim 4$  km.  
122 Some of these mafic rocks are highly deformed mylonites, whereas some just show slight traces of  
123 metamorphism. In this study, we focus on zircon U-Pb ages of magmatic rocks from this Cadomian  
124 section and particularly on the cumulate rocks as a likely “deep crustal MASH zone” that was responsible  
125 for generating Cadomian middle-upper crust felsic rocks associated with an  $\sim 10$  Ma long Cadomian arc-  
126 crust generation in NE Iran.

## 127 **Analytical methods**

128 Twelve new LA-ICPMS and SIMS zircon ages and Lu-Hf isotope data are reported on middle to  
129 lower crustal intrusions, both cumulates and their metamorphic equivalents (metagabbros, mylonitic  
130 gabbros and amphibolites) as well as granitic to tonalitic gneisses. We analyzed five samples (those dated  
131 by LA-ICPMS) for zircon trace elements and used these data to carry out Ti-in-zircon thermometry.  
132 Whole-rock major- and trace elements and Sr-Nd-Pb isotopes, and the compositions of minerals in  
133 magmatic rocks are also presented. We used also Electron Back-Scatter Diffraction analysis to investigate  
134 the deformation regime of the studied rocks. Analytical procedures are described in Appendix A.

## 135 **Results**

### 136 *Sample descriptions*

137 Field work and sample collection were done on felsic to intermediate metamorphosed intrusions and  
138 dikes from the upper-middle crust and on lower crustal cumulate rocks from the area NE of Torud (NE

139 Iran, Fig. 1). The new data presented here are integrated with other data from Cadomian terranes of NE  
140 Iran ([Moghadam et al., 2015](#)).

141 Cadomian cumulate rocks from NE Iran include gabbronorites (olivine + clinopyroxene; Cpx +  
142 orthopyroxene; Opx + plagioclase ± spinel), metagabbros (Cpx + amphibole + plagioclase ± olivine ±  
143 Opx ± garnet ± quartz ± phlogopite), amphibolites (amphibole + plagioclase ± Cpx ± quartz ± K-feldspar)  
144 and metapyroxenites (olivine + altered Cpx + titanomagnetite). Granitic (now granitic gneiss) dikes  
145 crosscut these rocks and include quartz + K-feldspar + plagioclase ± garnet ± biotite. Middle-crustal  
146 metamorphosed intrusions and their crosscutting dikes comprise granitic to tonalitic gneisses. These rocks  
147 contain K-feldspar (orthoclase and microcline) + quartz + plagioclase + biotite ± garnet ± amphibole ±  
148 muscovite ± allanite. The detailed petrographic composition of the sampled rocks is presented in Table  
149 S1.

150 Symplectites are present between olivine and plagioclase in metagabbros and comprise thin bands of  
151 Opx and thick bands of amphibole (Figs. 2A-S1A). Vermicular garnet is present within the amphibole  
152 corona (Figs. 2B-S1B). Plagioclase in gabbronorites is slightly zoned (Figs. 2C-S1C) and shows a thin  
153 amphibole corona at the contact with olivine (Figs. 2D-S1D). Plagioclase from mylonitic gabbros shows  
154 slight patchy zonation (Figs. 2E-S1E). Garnets in granitic gneisses are not zoned and include grains of  
155 quartz and amphibole (Figs. 2F-S1F).

156 Granitic gneisses and gabbros reveal varying degrees of deformation. A granitic gneiss (SH16-  
157 28) displays highly deformed quartz coexisting with less deformed feldspars. The c-axis distribution  
158 (obtained using Electron Back-Scatter Diffraction analysis; -EBSD) indicates deformation of quartz by  
159 dislocation creep with significant shear strain (Fig. S3A). A mylonitic gabbro (sample SH16-42) shows  
160 relics of deformed clinopyroxenes surrounded by coarse-grained deformed amphibole crystals (Fig. S3B).  
161 Fine-grained, internally-equilibrated amphiboles grew at the expense of large amphiboles. This  
162 microstructure indicates deformation of early clinopyroxenes which were then replaced by amphibole.  
163 Subsequent deformation is evidenced by a reduction in amphibole grain size and development of a  
164 foliation.

#### 165 *Mineral compositions*

166 Clinopyroxene from cumulate gabbros is augite (Fig. S2A) with Mg# ~0.8. Orthopyroxene has high  
167 Al<sub>2</sub>O<sub>3</sub> contents (1.3 to ~2 wt%; Table S2). Olivine has forsterite contents of 69-77%. Cumulate  
168 plagioclase has labradorite to bytownite composition, whereas metagabbros and mylonitic gabbros have  
169 more sodic plagioclase, in the range of oligoclase-andesine (Fig. S2B). Granodioritic gneisses contain  
170 plagioclase with andesine composition. Most amphibole cumulates (and their metamorphic equivalents)  
171 are characterized by high-Al (Al<sub>2</sub>O<sub>3</sub>=10-15 wt%) pargasitic and magnesio-hornblende compositions, but  
172 edenitic and tschermakitic compositions are also common (Fig. S2C). Garnet from mylonitic gabbros has

173 high contents of almandine (55.7%) and grossular (38%) but low pyrope (2.1%) and spessartine (4.1%)  
174 endmembers, whereas granitic gneisses have garnets with slightly higher almandine (~56-58%). Garnet in  
175 granodioritic gneisses has almandine endmember in the range of 49.3 to 67.7%. Mica in granitic gneisses  
176 is biotite (Mg# ~ 0.2-0.3), whereas mylonitic gabbros carry phlogopite (Mg# ~0.8). Spinels are  
177 ferritchromite with high FeO (37-66 wt%) and Cr# 0.2-0.4 (Table S2).

#### 178 *Zircon U-Pb dating and Hf isotope*

179 Figures 3 and 4 show the LA-ICPMS and SIMS U-Pb zircon ages obtained in this study for two  
180 Cadomian metagabbros, one metagabbronorite, one mylonitic gabbro, one granitic (-gneiss) dike within  
181 metagabbros, one hornblende-bearing metagabbro, one tonalitic gneiss, four granitic to granodioritic  
182 gneisses and one granitic (-gneiss) dike within granodioritic gneisses. Details of the U-Pb geochronology  
183 are provided below.

#### 184 *Sample SH16-28:*

185 This sample is a garnet-bearing granitic gneiss, injected within the Cadomian metagabbros. The  
186 sample contains porphyroblasts of quartz, K-feldspar, plagioclase, biotite and garnet. CL images of  
187 zircons revealed neither inherited cores nor metamorphic rims. Zircons are ~150-100  $\mu\text{m}$  long. Most  
188 zircons have oscillatory zoning. Zircons separated from this sample contain 115-1713 ppm U, 276-1394  
189 ppm Th and Th/U = 0.2-0.8. We analyzed 38 zircon grains from this sample (Table S3A). The twenty-  
190 seven analyses are concordant (Fig. 3) and yield a mean  $^{206}\text{Pb}/^{238}\text{U}$  age of  $537.7 \pm 2.6$  Ma (MSWD = 1.3).  
191 This is taken as the crystallization age of this granitic dike. Some zircons have  $^{206}\text{Pb}/^{238}\text{U}$  ages of 541 to  
192 566 Ma (and one grain with 669 Ma) and are considered as antecryst and xenocrystic zircons.

193 Sample SH16-28 displays a notable range of  $\epsilon\text{Hf}$ , between -3.4 and -24.7 (Table S5). Corresponding  
194 crustal model ages ( $T_{\text{DM}}^{\text{C}}$ ) for zircons from sample SH16-28 vary from 1.7 to 3 Ga.

#### 195 *Samples SH16-14 and SH16-43:*

196 These samples are metagabbros with relict plagioclase, amphibole and clinopyroxene. Zircons  
197 separated from these samples are large ( $>100$   $\mu\text{m}$  in sample SH16-43) or short prismatic (~70-100  $\mu\text{m}$  in  
198 sample SH16-14) and most show oscillatory zoning. Zircons contain 186-4395 ppm U, 159-11666 ppm  
199 Th contents and Th/U from 0.3-4.7 (Table S3A). Some zircons have high Th and U content. Out of thirty-  
200 five zircon grains analyzed for both samples, twenty-two grains yield a mean  $^{206}\text{Pb}/^{238}\text{U}$  age of  $542.1 \pm$   
201  $2.5$  Ma (MSWD = 1.5; Fig. 3) for sample SH16-14 and twenty-one zircons give a mean  $^{206}\text{Pb}/^{238}\text{U}$  age of  
202  $534.3 \pm 2.1$  Ma (MSWD = 2). These ages (~542-534) are taken as the crystallization age of the gabbros.  
203 Some other zircons show  $^{206}\text{Pb}/^{238}\text{U}$  ages of  $> 547$  Ma and up to 624 Ma, which are considered as both  
204 antecryst and inherited zircons. Samples SH16-43 include few zircons with high U and Th contents,  
205 which these zircons show younger ages of 505 and 509 Ma. We have deleted these younger ages from age  
206 interpretation of this sample, as they probably are related to destruction of the zircon structure due to the

207 high U and Th abundances.

208 Sample SH16-43 displays a noticeable range of  $\epsilon_{\text{Hf}}$ , between +2.7 and +9.2 (Table S5).

209 Corresponding crustal model ages ( $T_{\text{DM}}^{\text{C}}$ ) for zircons from sample SH16-43 vary from 0.9 to 1.3 Ga.

210 Sample SH16-14 has zircon  $\epsilon_{\text{Hf}}$  ranging from +6.9 to -0.2, lower than the  $\epsilon_{\text{Hf}}$  values of zircons in sample

211 SH16-43. Corresponding  $T_{\text{DM}}^{\text{C}}$  for zircons from sample SH16-14 vary from 1.1 to 1.5 Ga.

212 *Sample SH16-17:*

213 This sample is a foliated hornblende-bearing metagabbro. The sample contains coarse-grained relict

214 amphibole, plagioclase, quartz with clinopyroxene. CL images of zircons revealed neither inherited cores

215 nor metamorphic rims. Zircons are short prismatic, and ~50-70  $\mu\text{m}$  long. Most zircons are homogenous

216 and lack oscillatory zoning, except in the grains' rims. Zircons separated from this sample contain 279-

217 2642 ppm U, 222-7281 ppm Th and Th/U= 0.7-3.5. We analyzed 35 zircon grains (Table S3A). Zircons

218 are concordant or near concordant (Fig. 3) and yield a mean  $^{206}\text{Pb}/^{238}\text{U}$  age of  $536.8 \pm 2.4$  Ma (MSWD =

219 1.9). This is taken as the crystallization age of this hornblende-bearing metagabbro. Sample SH16-17 has

220 zircon  $\epsilon_{\text{Hf}}$  values ranging from +6.5 to -7.9, more variable than the  $\epsilon_{\text{Hf}}$  values of other gabbroic zircons.

221 Corresponding  $T_{\text{DM}}^{\text{C}}$  for zircons from sample SH16-17 vary from ~ 1.1 to 2 Ga.

222 *Sample SH16-42:*

223 This sample is a highly deformed mylonitic metagabbro. It contains relict amphibole, plagioclase,

224 clinopyroxene, with quartz and garnet. There are neither inherited cores nor metamorphic rims in zircon

225 grains of this sample. Zircons are short-medium prismatic ~70-100  $\mu\text{m}$  long. Most zircons display some

226 oscillatory zoning. Z

227 The zircons contain 422-2833 ppm U, 277-4289 ppm Th and Th/U= 0.6-1.5. We analyzed 23 zircon

228 grains from this sample (Table S3A). The nineteen analyses yield a mean  $^{206}\text{Pb}/^{238}\text{U}$  age of  $531.9 \pm 2.4$  Ma

229 (MSWD = 1.6) (Fig. 3). This is taken as the crystallization age of this gabbroic rock. Zircons from sample

230 SH16-42 displays a narrow range of  $\epsilon_{\text{Hf}}$ , between +3.1 and -0.1 (Table S5). Corresponding  $T_{\text{DM}}^{\text{C}}$  for

231 zircons from sample SH16-42 vary from 1.5 to 1.3 Ga.

232 *Sample SH16-34:*

233 This sample is taken from Torud gabbro-norites and contain olivine, Cpx, Opx and plagioclase.

234 Zircon grains from this sample are small, from ~50  $\mu\text{m}$ . Most crystals have magmatic zonation. Twenty-

235 four analyses are characterized by relatively moderate Th/U (~0.2-6.2) and low common lead ( $f_{206}$ , the

236 proportion of common  $^{206}\text{Pb}$  in total measured  $^{206}\text{Pb}$ , <1.3%) (Table S3B). All analyses are concordant

237 within analytical errors (Fig. 3), yielding a concordia age of  $541.8 \pm 2.9$  Ma on a  $^{206}\text{Pb}/^{238}\text{U}$  vs  $^{207}\text{Pb}/^{235}\text{U}$

238 diagram. The weighted mean  $^{206}\text{Pb}/^{238}\text{U}$  age of is  $541.6 \pm 3.3$  Ma. This age is interpreted as the

239 crystallization age of this sample. Zircon  $\epsilon_{\text{Hf}}$  values vary between +8.3 and -1.6 (Table S5).

240 Corresponding  $T_{\text{DM}}^{\text{C}}$  for zircons from sample SH16-34 vary from 0.9 to 1.6 Ga.

241 *Sample SH16-10:*

242 This sample is from tonalitic gneisses and contains plagioclase, amphibole and quartz with rare K-  
243 feldspar. Zircons are long prismatic (100-150  $\mu\text{m}$ ) and stubby with concentric and oscillatory zoning.  
244 Thirteen analyzed points show low Th/U of 0.2-0.6. Common lead ( $f_{206}$ ) is <0.6%. The analyzed zircons  
245 give a weighted mean  $^{206}\text{Pb}/^{238}\text{U}$  age of  $542.1 \pm 2.9$  Ma (MSWD = 0.9). Zircons from sample SH16-10  
246 display a narrow range of  $\epsilon\text{Hf}$ , between -2.6 and -6.1 (Table S5). Crustal model ages for zircons from  
247 sample SH16-10 vary from 1.7 to 1.8 Ga.

248 *Samples CHJ10-17, BJ11-26 and BJ11-27:*

249 These samples are taken from middle-crustal granodioritic gneisses and contain plagioclase, K-  
250 feldspar and quartz along with biotite and garnet. Zircons are mostly short to long-prismatic (>70  $\mu\text{m}$  to  
251 150  $\mu\text{m}$ ) and some have inherited cores. The analyzed spots (30 spots for each sample) have Th/U ratios  
252 of 0.1 to 0.6 with quite low common lead (nearly all zircons have  $f_{206}<1.9$ ). Analyzed zircons are  
253 concordant within analytical errors (Fig. 4) and yield weighted mean  $^{206}\text{Pb}/^{238}\text{U}$  ages of  $541.2 \pm 3.0$  Ma  
254 (MSWD= 0.9) for sample CHJ10-17,  $545.2 \pm 3.9$  Ma (MSWD= 1.6) for sample BJ11-26 and  $547.1 \pm 3.2$   
255 Ma (MSWD= 0.9) for sample BJ11-27. Some other zircons show  $^{206}\text{Pb}/^{238}\text{U}$  ages from > 560 Ma up to 1  
256 Ga and are considered to be inherited. Zircon  $\epsilon\text{Hf}$  values for granodioritic gneisses range from +2.1 to -  
257 13.8, but most zircons show negative  $\epsilon\text{Hf}$  ( $av = -3.4$ ). Corresponding  $T_{\text{DM}}^{\text{C}}$  for these zircons vary from 1.4  
258 to 2.3 Ga.

259 *Sample CHJ10-33:*

260 This sample is taken from a granitic dike within the granodioritic gneisses. The sample is  
261 metamorphosed and contains K-feldspar, quartz, plagioclase, garnet, biotite and muscovite. Zircons from  
262 this sample are large (~100-150  $\mu\text{m}$ ) prismatic. Thirty analyzed spots have Th/U ratios between 0.2 and  
263 0.7 (except one spot with Th/U=0.01). Common-lead contents are low in most grains; with  $f_{206} < 0.1\%$ .  
264 The analysed zircons yield a weighted mean  $^{206}\text{Pb}/^{238}\text{U}$  age of  $541 \pm 3.2$  Ma (MSWD=0.6). This age is  
265 interpreted as the timing of dike crystallization. One inherited core shows a  $^{206}\text{Pb}/^{238}\text{U}$  age of ~1 Ga.  
266 Zircon  $\epsilon\text{Hf}$  values for this granitic dike vary between +1.1 and -7.7, with  $T_{\text{DM}}^{\text{C}} = 1.4-1.9$  Ga.

267 *Sample BJ11-19:*

268 This is a granitic gneiss and contains K-feldspar, quartz and minor plagioclase. Zircons from this  
269 sample are coarse-grained (~150  $\mu\text{m}$ ). Twenty-seven SIMS analyses were obtained. The zircons show a  
270 weighted mean  $^{206}\text{Pb}/^{238}\text{U}$  age of  $544.6 \pm 3.5$  Ma (MSWD=1.2). Zircon  $\epsilon\text{Hf}$  values vary between +0.5 and  
271 -6.7, with  $T_{\text{DM}}^{\text{C}} = 1.5-1.9$  Ga.

272 *Thermobarometry*

273 The Ti-in-zircon thermometer ([Watson et al., 2006](#)) yields temperatures of 849-815  $^{\circ}\text{C}$  for gabbros,  
274 786  $^{\circ}\text{C}$  for mylonitic gabbros, 781  $^{\circ}\text{C}$  for metagabbros and 684  $^{\circ}\text{C}$  for granitic gneisses. These

275 temperatures are lower than those calculated using the Fe-Mg ratios ( $K_D$ ) of two equilibrated pyroxenes in  
276 gabbronorites (sample SH16-9; 1025 °C) or the Ca-in-Opx thermometer (1236 °C) ([Brey and Köhler,](#)  
277 [1990](#)). The pressure calculated from amphibole geochemistry using the barometers of ([Hammarstrom and](#)  
278 [Zen, 1986](#)) and ([Schmidt, 1992](#)) is 8 kbar for metagabbros, 7.5 for gabbronorites and 5.7 kbar for gabbros,  
279 corresponding to depths of ~26 km, 25 km, and 19 km, respectively. A geothermal gradient of 30-  
280 45°C/km is calculated from these data.

### 281 *Cumulate geochemistry*

282 The Cadomian cumulates of NE Iran have low to moderate Mg# (29-50) with 46 to 55 wt % SiO<sub>2</sub>  
283 and 13.2 to 17.3 wt % Al<sub>2</sub>O<sub>3</sub>. TiO<sub>2</sub> contents are low; 0.5-1.1 wt %. These rocks are quite enriched in light-  
284 rare earth elements (LREEs) ( $La_{(n)}/Yb_{(n)} = 1.9-7.8$ , normalized to N-MORB). The rocks are also enriched  
285 in incompatible elements such as Cs, Rb, Ba, Th, U, K and Pb but are depleted in Nb, Ta and Zr relative  
286 to the LREE, as is typical for arc-related igneous rocks (Fig. 5A). Mid-crustal felsic intrusions have high  
287 SiO<sub>2</sub> (74.1-76.5 wt%) but lower MgO (0.1-0.4) and Al<sub>2</sub>O<sub>3</sub> (12.4-13). These rocks are enriched in LREEs  
288 with  $La_{(n)}/Yb_{(n)} = 8.3-34.9$ . Positive anomalies in Cs, Rb, Ba, Th, U, K and Pb and depletion in Nb-Ta and  
289 Ti are conspicuous (Fig. 7A).

290 Cumulate rocks analyzed for Sr-Nd and Pb isotopes have variable initial  $^{87}Sr/^{86}Sr_{(t)}$  (0.703-0.709) and  
291  $\epsilon Nd(t)$  values (-1.3 to +3.4). Initial  $^{206}Pb/^{204}Pb_{(t)}$  and  $^{208}Pb/^{204}Pb_{(t)}$  isotope ratios for these rocks vary from  
292 18.14 to 18.55 and 38.21 to 38.85, respectively.  $^{208}Pb/^{204}Pb_{(t)}$  ratios for these rocks are similar to pelagic  
293 limestones, whereas the  $^{207}Pb/^{204}Pb_{(t)}$  ratios for cumulates are high (15.71 to 15.76) and are similar to  
294 upper continental crust (Fig. 5B-C).

295

### 296 **Discussion**

297 There are five main questions concerning NE Iran Cadomian cumulates and associated rocks. First,  
298 what is the timescale of magmatic build-up in the Cadomian crust of NE Iran? Second, did these cumulate  
299 form in a Cadomian deep crustal hot zone? Third, did differentiation (or assimilation-fractional  
300 crystallization=AFC) generate the middle-upper crust felsic rocks? Fourth, what caused the intense  
301 deformation in some of these rocks? Finally, what was the relationship between the deep crustal hot zone  
302 and the Cadomian magmatic flare-up? These questions are addressed below.

### 303 *Repeated magmatic build-up*

304 The summary of new zircon U-Pb age data shows gabbro cumulates have mean zircon  $^{206}Pb/^{238}U$   
305 ages of 542 to 534 Ma whereas a mylonitic gabbro has an age of 532 Ma. Gabbronorites have mean  
306  $^{206}Pb/^{238}U$  ages of 542 Ma, suggesting that mafic magmatism continued at least from ~ 542 to 532 Ma  
307 (~10 Myr). Mid-crustal intermediate to felsic intrusions and felsic dikes have mean  $^{206}Pb/^{238}U$  ages of 547  
308 to 538 Ma (~9 Myr). Mid-crustal intrusions have older ages of ~547 Ma, but their ages also overlap with

309 the crystallization of mafic cumulates (Fig. 6). This shows that younger mafic inputs were occurring  
310 while the more evolved portions of the middle crust of the arc were being established. These new data  
311 also indicate that the arc crust was constructed by magmatic build-up over a ~15 Myr time scale.  
312 However, previously-published zircon U-Pb data on the middle-upper crustal intrusions and  
313 metasediments show ages of 561 to 530 Ma, a much longer magmatism (~31 Myr). In addition, zircon U-  
314 Pb data attest that the Cadomian magmatism in Iran and Anatolia start at ~620 Ma and ended at 500 Ma.  
315 However, this ~120 Myr magmatic ignition seems to be spatially variable across different Cadomian arc  
316 segments in Iran and Anatolia. Continentally retreating arcs usually have an average lifespan of ~100  
317 Myr, while oceanic arcs live for ~40 Myr ([Ducea et al., 2015a](#)). Extensional arcs such as the Cadomian  
318 arcs seem to be quite longer (~120 Myr).

319 Cadomian magmatic pulses from NE Iran seem to have different Hf-isotopic compositions. The  
320 initial  $^{176}\text{Hf}/^{177}\text{Hf}$  ratio of zircon from metagabbros ranges from  $\epsilon\text{Hf}(t) = -7.9$  to  $+9.2$  ( $av = +3.6$ ); a younger  
321 gabbro (sample SH16-43; 534 Ma) has more radiogenic Hf than the older gabbro sample (542 Ma).  
322 Sample SH16-17 has zircons with variable, but less radiogenic Hf isotopic compositions ( $\epsilon\text{Hf}(t) = -7.9$  to  
323  $+6.5$ ). Zircons from middle crust intrusions and dikes have variable  $\epsilon\text{Hf}(t)$  of  $-27.7$  to  $+5.4$  ( $av = -4$ ). New  
324 zircon Lu-Hf isotope data highlight middle crust felsic intrusions have less radiogenic Hf isotope than  
325 deep gabbro cumulates.

#### 326 *Crustal profile and deep “hot zone”*

327 In the “deep crustal hot zone” model, mantle-derived hydrous basaltic magmas are emplaced into the  
328 lower crust over a few million years as a succession of sills ([Annen et al., 2006](#)). Crustal “hot zones” are  
329 regions where MASH processes occur; they have been recognized in both continental arcs with thick  
330 crust (e.g., Andes, ([Annen et al., 2006](#))) and intra-oceanic arcs with thin crust (e.g., Izu-Bonin-Mariana,  
331 ([Stern et al., 2019](#))).

332 Partial crystallization of basaltic melts in the deep hot zones and interaction with surrounding rocks  
333 generates residual and anatectic H<sub>2</sub>O-rich melts. These H<sub>2</sub>O-rich melts and the heat released from the  
334 crystallizing magmas in turn promote partial melting of the adjacent pre-existing continental crust.  
335 Mixing of the H<sub>2</sub>O-rich residual melts, primitive melts, and crustal melts leads to the diverse chemical  
336 and isotopic compositions of the resultant secondary magmas.

337 Cadomian igneous rocks formed along an active continental margin, with high fluxes of magmatism  
338 (“flare-up”) in Ediacaran time ([Moghadam et al., 2017d](#)). Above this Neoproterozoic subduction zone,  
339 melting in the mantle wedge produced mafic magmas, which rose and stalled in the lower crust. The  
340 primary mantle melt that formed the Cadomian lower-crustal cumulates seems to have been a magnesian  
341 andesite (gabbroonorite) because it crystallized both olivine and orthopyroxene. This melt had moderately

342 low  $p\text{H}_2\text{O}$ , so that it first crystallized anhydrous phases (olivine and Opx) and plagioclase with quite low  
343 anorthite contents. Only later did water contents become high enough to crystallize amphibole.

344 Incomplete differentiation of these early, high-Mg phases in a deep-arc crustal hot zone produced  
345 silica-rich residual melts, which fractionated in shallower magma chambers and assimilated older  
346 continental crust, to produce the granitoids that dominate the upper crust. Such shallow magma chambers  
347 solidified to form syn-tectonic granitoids and granitoid gneisses at depth and undeformed plutons at  
348 higher levels. In support of this overall scenario, lower-crustal rocks also have more juvenile zircon Hf  
349 (and whole rock Nd) isotope signatures than do shallower, more evolved igneous rocks. The middle-upper  
350 crustal rocks are affected by greater assimilation of pre-existing country rocks, whereas mafic rocks show  
351 a minor contribution of crustal components. The crustal isotopic (bulk rock Nd-Pb and zircon Hf)  
352 signature of the NE Iran gabbroic rocks can plausibly be attributed in part to a “contaminated” mantle  
353 source, in which the lithospheric mantle was already contaminated by crustal materials; either by lower  
354 crustal delamination or by subduction erosion ([Lackey et al., 2005](#)).

355 Figure 6 shows that bulk rock  $\text{SiO}_2$  and Zr increase from lower-crustal cumulates to upper-crustal  
356 intrusions, whereas CaO decreases, showing the importance of fractionation of early-crystallized minerals  
357 for magmatic evolution. Plots of trace elements on a N-MORB normalized diagram (Fig. 5) indicate that  
358 magmatic fractionation dominated, leading to major negative anomalies in some elements such as Ti and  
359 enrichment in other incompatible elements such as Zr and HREEs in fractionated middle-upper crustal  
360 rocks compared with the lower-crustal cumulates. The range of zircon Hf and bulk rock Nd isotopic  
361 compositions suggest that AFC was also important. We infer that a hot zone in the middle and lower crust  
362 was responsible for forming the more evolved magmas that now comprise the rocks of the Cadomian  
363 middle to upper crust of NE Iran.

364 A crustal profile of the Cadomian arc of Iran has been reconstructed by using Sr/Y elemental ratios  
365 for intermediate rocks ([Chapman et al., 2015](#)) and Ce/Y ratios for mafic rocks ([Mantle and Collins, 2008](#)).  
366 ([Chapman et al., 2015](#)) suggested that Sr/Y can be used as a proxy for crustal thickness intermediate calc-  
367 alkaline rocks (55-68 wt%  $\text{SiO}_2$ ). Our compiled data show that most Cadomian rocks with intermediate  
368  $\text{SiO}_2$  composition show a crustal thickness of 20 to 30 km. Gabbroic cumulates (*this study*) have  
369 maximum Ce/Y ratios <1.4, indicating a crustal thickness for the Iran Cadomian arc of <30 km.  
370 Amphibole-Al geobarometry also records an emplacement depth of 19-26 km for the metagabbros, just  
371 above the Cadomian Moho beneath NE Iran.

#### 372 *FC-AFC processes and generation of the Cadomian arc crust*

373 Fractional crystallization (FC) and coupled Assimilation-Fractional Crystallization (AFC) models  
374 can be used to test the hypothesis that Cadomian middle-upper crust felsic rocks are differentiated melts  
375 from a mafic parental melt. Based on mineral- and whole rock chemistry, a gabbroic melt (sample SH16-9)

376 and a hornblende-bearing metagabbro (sample SH16-17) were selected as best approximations to parental  
377 magma compositions.

378 Major-element mass-balance models show that the studied gabbroic rocks ( $\text{SiO}_2 < 52$  wt%, lower  
379 and middle crust mafic intrusions) reflect 30-67% fractional crystallization of gabbronoritic parental melts  
380 with a crystallizing assemblage of clinopyroxene, plagioclase, olivine and ilmenite ( $\text{Cpx}_{2.3-13.3} + \text{Pl}_{26.5-40.8} +$   
381  $\text{Ol}_{49.4-59.9} + \text{Ilm}_{<2}$ ; hereafter percentages are given for the total crystallized assemblage). Approximately  
382 75-92% fractional crystallization of a similar assemblage ( $\text{Cpx}_{11.7-14.2} + \text{Pl}_{41.5-42.3} + \text{Ol}_{41.5-54.9} + \text{Ilm}_{<2}$ ), can  
383 produce higher-silica ( $\text{SiO}_2 > 52$  wt.%) lower and middle crust mafic intrusions (metagabbros, gabbros  
384 and diorites) from the same gabbronoritic (SH16-9) parental melt. Moreover, differentiation of  
385 gabbronoritic melt to form middle and upper crust felsic rocks can result from 91-94% fractional  
386 crystallization of the previous assemblage ( $\text{Cpx}_{13-16.3} + \text{Pl}_{40.1-43.0} + \text{Ol}_{41.1-42.2} + \text{Ilm}_{1.8-2.2}$ ). However, these  
387 fractionating assemblages fail to reproduce all upper crust felsic rocks (granites and rhyolites) and the  
388 overall differentiation trend ( $\sum r^2 > 1.0$ ), mainly due to the large  $r^2$  for Ti, Fe, Mg and Ca, suggest either  
389 the presence of another concurrent fractionating assemblage, or assimilation of crustal material. Crustal  
390 assimilation is also indicated by the variable isotope signatures of the rocks.

391 Given the presence of Ca-amphibole in the gabbroic rocks, mass balance models have been  
392 recalculated for an assemblage with hornblende ( $\text{Cpx} + \text{Pl} + \text{Hbl} + \text{Ilm}$ ). Model solutions show that  
393 Cadomian intermediate and felsic rocks ( $\text{SiO}_2 > 54$  wt.%) could be the result of 72-85% fractional  
394 crystallization of Hbl gabbros (sample SH16-17) with an assemblage of clinopyroxene, plagioclase,  
395 hornblende and ilmenite ( $\text{Cpx}_{0.5-4} + \text{Pl}_{12.1-24.3} + \text{Hbl}_{66.8-86.3} + \text{Ilm}_{1.8-2.1}$ ). Even if the hornblende-bearing  
396 assemblage is more efficient in producing upper- crustal rhyolites, these mass balance models again fail to  
397 reproduce the middle and upper crust felsic intrusions ( $\sum r^2 > 1.0$ ) due to the large  $r^2$  for Fe, Mg and K,  
398 further indicating that crustal assimilation accompanied fractional crystallization (e.g. ([McBirney et al.,](#)  
399 [1987](#))) to produce high- $\text{SiO}_2$  melts.

400 A Harker-like plot for major element mass-balance FC and AFC models is presented in Fig. 7. FC  
401 trends are reported for three representative fractionating assemblages: i) *O11* ( $\text{Cpx}_{2.6} + \text{Pl}_{40.8} + \text{Ol}_{54.9} +$   
402  $\text{Ilm}_{1.6}$ ), ii) *O12* ( $\text{Cpx}_{14.0} + \text{Pl}_{42.6} + \text{Ol}_{41.3} + \text{Ilm}_{2.1}$ ) and iii) *Hbl* ( $\text{Cpx}_{3.0} + \text{Pl}_{20.8} + \text{Hbl}_{74.5} + \text{Ilm}_{1.7}$ ). Lever-rule  
403 models to visualize the AFC processes for the gabbroic parental melts and Cadomian upper-crustal  
404 sediments, could represent the maximum interaction/assimilation effect. The assimilation processes were  
405 dominant and generated residual liquids in the compositional space between the maximum assimilation  
406 trend and a minimum trend, represented by the pure FC curves (i.e. assimilation = 0).

407 Based on the major-elements FC-AFC solutions, we re-calculated the FC-AFC trends using trace  
408 elements (La, Yb, Nb and Y) to further investigate the major role of fractionating assemblages such as  
409 Ca-plagioclase, Ca-hornblende and Mg-olivine (Fig. 8).

410 The results for the trace elements are consistent with the major-element models and further support  
411 the FC-AFC model. FC-models calculated for olivine-bearing assemblages (O11 and O12) suggest that the  
412 lower- and middle-crustal mafic intrusions (i.e. gabbros and metagabbros) were produced by 40-60%  
413 fractional crystallization of the parental melts.

414 FC-curves (maximum and minimum) calculated for both olivine- (O11 and O12) and hornblende-  
415 bearing (Hbl) assemblages indicate that most granitoid rocks (upper- to middle-crust felsic intrusions) are  
416 not the products of pure fractional crystallization from a mafic parental melt (neither gabbro nor  
417 hbl-metagabbro). However, a combination of fractional crystallization (FC 40-90%) and concurrent  
418 assimilation of ~20% (*proportion of assimilant to fractionates* = 0.2) of Cadomian upper-crustal  
419 sediments could produce most Cadomian felsic rocks. This supports the presence of a deep crustal hot  
420 zone and its role in forming nearly all Cadomian magmatic rocks of Iran via FC-AFC processes from  
421 mafic parental melts.

#### 422 *Deep arc crust and deformation*

423 The above calculations imply that the Cadomian flare-up magmatism must have generated a dense  
424 root of ultramafic-mafic cumulates, 3-4 times as voluminous as the present Iranian crust. There is no  
425 evidence for the presence of such a thick root beneath Iran today, and it may have foundered into the  
426 mantle ([Ducea, 2002](#)), perhaps even during the magmatic flare-up, when the lower crust is hottest and  
427 weakest and the largest volumes of dense cumulates are produced. The preservation of thick cumulates in  
428 the lower crust of arcs is unusual, as they commonly either delaminate after the flare-up event or are  
429 tectonically removed during the later plate tectonic movements ([Chapman et al., 2016](#)). Garnet-rich  
430 cumulates are especially dense and prone to sinking, and it is likely that the shallow limit of garnet  
431 stability (~30 km) made it impossible to thicken the Iran-Anatolia Cadomian crust beyond this.

432 Besides the missing volume of mafic-ultramafic cumulates, there may be other evidence of  
433 Cadomian lower-crustal foundering. The occurrence of metamorphic coronas between olivine and  
434 plagioclase with fine-grained vermicular garnet crystals and the presence of garnet in mylonitic gabbros  
435 attest to a phase of high-grade metamorphism and intense deformation that may have occurred during  
436 foundering of cumulates. The EBSD images from mylonitic gabbros also record strong deformation of  
437 early-crystallized clinopyroxenes and coarse-grained amphiboles. Most coronas between olivine and  
438 plagioclase contain layers of orthopyroxene and amphibole  $\pm$  spinel suggesting partial re-equilibration in  
439 the presence of a fluid-rich phase ([Otamendi et al., 2010](#)), but in more complex cases garnet is seen near  
440 reactant plagioclase. The occurrence of highly deformed amphibole associated with clinopyroxene relics  
441 may indicate protracted polybaric crystallization involving a second H<sub>2</sub>O-rich melt (H<sub>2</sub>O > 4 wt%), which  
442 was cool enough (<1000 °C) to stabilize amphibole ([Muntener et al., 2001](#)). This seems to have happened

443 deep in the arc crust, as indicated by the high  $\text{Al}_2\text{O}_3$  content and strong deformation of the paragonitic  
444 amphiboles.

#### 445 *Tempo of Cadomian arc magmatism*

446 The Cadomian arcs of Iran-Anatolia were important sites of continental growth, with the bulk of  
447 igneous rocks being emplaced during the Ediacaran flare-up. This magmatic flare-up was responsible for  
448 forming ~30 km of Cadomian crust in Iran-Anatolia, consisting of gabbroic cumulates, variably  
449 metamorphosed mafic to felsic intrusions and felsic volcanic-pyroclastic rocks (Fig. 9A). The existence of  
450 mafic and felsic magmatic rocks among the Cadomian outcrops indicates bimodal magmatic activity (Fig.  
451 9), which is well known from modern intra-oceanic and Andean-type arcs (e.g., [Ducea et al., 2015a](#);  
452 [Stern et al., 2014](#)). Some estimate that the generation of such large volumes of crust requires about 50%  
453 from melting of lower continental crust and lithospheric mantle and 50% from melting of the  
454 metasomatized mantle wedge above the subducting oceanic slab ([DeCelles et al., 2009](#); [Ducea et al.,](#)  
455 [2015a](#)). Plutonism is the principle expression of magmatic flare-ups, with ratios of plutonism to  
456 volcanism estimated as high as ~30:1 ([Paterson and Ducea, 2015](#)). The Cadomian arcs of Iran-Anatolia  
457 (and perhaps Europe, SW Asia, and E. North America) record abundant plutonism and significant  
458 volcanism accompanying crustal thickening and long-lived magmatism involving melting of both mantle  
459 and overlying continental crust ([Moghadam et al., 2017d](#)). Although our new data on Cadomian crust of  
460 NE Iran indicate a ~15 Myr prolonged magmatic activity, but our compiled zircon U-Pb data on  
461 Cadomian magmatic rocks of Iran demonstrate an intense episode of magmatic activity that lasted ~45  
462 Myr, from 570 to 525 Ma (Fig. 9B), involving magmas with different geochemical signatures and  
463 isotopic disturbances (Figs. 9F-G) ([Moghadam et al., 2017d](#)). The most obvious products of the  
464 Cadomian flare-up are the igneous rocks of the upper crust: felsic plutons and volcanics (Figs. 9C & E).  
465 In spite of this, it was mafic magmatism that powered the flare-up episode, and similar magmas also  
466 prevail during episodes of normal arc magmatism (Fig. 9D). There is no evidence for repeated flare-up  
467 episodes in SW Asia Cadomian arcs. The flare-ups may have halted when plate motions changed, leading  
468 to opening of a back-arc basin that grew into the Rheic Ocean. Uplift and erosion related to this supplied a  
469 thick sequence (>1000 m) of detrital sediments in Iran and Anatolia, which were predominantly (>90%)  
470 derived from erosion of Cadomian igneous rocks ([Moghadam et al., 2017c](#)).

471 The 40 Myr flare-up stage was characterized by an increase of magmatic flux rates by >3 orders of  
472 magnitude, compared to the “steady-state” flux, coupled with a significant disturbance in Sr-Nd-Hf  
473 isotope ratios (Figs. 9F-G) and a major contribution of pre-existing crustal rocks through AFC processes.  
474 The flare-up completely obliterated these older rocks; the only traces of their existence are found in the  
475 isotopic compositions of igneous rocks and in detrital zircons in sediments. In the Cadomian arcs of Iran  
476 and Anatolia, the inheritance ages are dominated by *ca* 1.3-1.4 and 2.5 Ga zircons ([Moghadam et al.,](#)

477 [2017d](#)), which is consistent either with the presence of as-yet undiscovered older Gondwanan crust or  
478 recycling of sediments through the arc system. Influx of asthenospheric materials to the arc root, due to  
479 the foundering of dense cumulates, may trigger the generation of more mafic magmas. This process has  
480 been suggested to explain the isotopic disruption of magmatic rocks from other arcs (e.g., ([Paterson and](#)  
481 [Ducea, 2015](#); [Stuart et al., 2016](#))).

482

### 483 **Conclusions**

484 Cadomian arcs of Iran and Anatolia is viewed as an “Andean” arc because it was emplaced within an  
485 old craton, although their extensional behavior makes them different than Andean arcs. Our new zircon  
486 U-Pb ages indicate that the Cadomian arc crust of NE Iran was built during ~15 Myr, similar to some  
487 modern arcs. However, all compiled data from Cadomian exposures in Iran and Anatolia show  
488 magmatism started at 620 Ma and ended at ~500 Ma with a flare-up period for ~45 Myr (570-525 Ma).  
489 This shows the magmatism was temporarily and spatially different at various section of the Cadomian arc.  
490 Cadomian arcs was intruded by voluminous mafic magmas that differentiated, generating intermediate  
491 melts that then interacted with variable amounts of middle-upper crust sediments to produce middle-upper  
492 crust felsic intrusions.

493 Our data show that the Cadomian magmatism in Iran and Anatolia was characterized by a period of  
494 high magmatic addition ( $>300 \text{ km}^3 \text{ km}^{-1} \text{ yr}^{-1}$ ), which seems to be related to a phase of high arc migration  
495 rate across Prototethyan trench (or roll-back). This made an extreme extension in the overlying  
496 continental crust of the subduction system, resulted in a flare-up episode. Thick arcs, such as the  
497 Cadomian arc of Iran and Anatolia are also characterized by dense cumulate build-up in lower crust,  
498 which can reduce the magmatic intensity into a lull period. Long-lived arcs or those which are under  
499 flare-up have higher mafic-ultramafic cumulates and then thicker roots ( $>30 \text{ km}$ ).

### 500 **Acknowledgments**

501 This study was funded by the “National Key Research and Development Program of China  
502 (2016YFE0203000)” and by “Chinese Academy of Sciences, President’s International Fellowship  
503 Initiative (PIFI, 2019VCB0013)”. This study used instrumentation funded by ARC LIEF and DEST  
504 Systemic Infrastructure Grants, Macquarie University, NCRIS AuScope and Industry. This is contribution  
505 xxx from the ARC Centre of Excellence for Core to Crust Fluid Systems (<http://www.cafs.mq.edu.au>),  
506 xxxx in the GEMOC Key Centre (<http://www.gemoc.mq.edu.au>), and UTD Geosciences contribution  
507 number xxxx. The authors acknowledge the facilities, and the scientific and technical assistance of the  
508 Australian Microscopy & Microanalysis Research Facility at the Electron Microscope Unit, The  
509 University of New South Wales, Australia. This paper benefited from discussion and advice from J.C.  
510 White. All logistical supports for the field work come from Damghan University.

511

512 **Figure captions**

513 Figure 1- A- Simplified geological map of Iran showing the distribution of Cenozoic igneous rocks,  
514 Mesozoic ophiolites, Paleozoic-Mesozoic igneous rocks and Cadomian basement rocks; the location of  
515 the study area is also shown. Cadomian basement makes up most of the crust of Iran. Modified from  
516 ([Moghadam et al., 2017a](#)) with John Wiley and Sons Inc. permission. B- Simplified geological map of  
517 NE Iran (Modified after 1/250,000 geological maps of Kharturan and Torud, Geological Survey of Iran).

518

519 Figure 2- Back-scattered images showing the symplectite overgrowths between olivine and plagioclase  
520 (in sample SH16-34), which composed of orthopyroxene and amphibole (A) with fine-grained vermicular  
521 growth of garnet (B). Zoned plagioclase from metagabbros (sample SH16-9) (C) with amphibole corona  
522 between olivine and plagioclase (D). Undeformed plagioclases from mylonitic gabbros (E) and garnet  
523 porphyroclasts (F) from gneissic granites. Garnets contain quartz and amphibole inclusions.

524

525 Figure 3- LA-ICPMS U-Pb concordia and mean  $^{206}\text{Pb}/^{238}\text{U}$  age plots for the Cadomian metagabbros,  
526 hornblende-bearing metagabbros, mylonitic gabbros and granitic gneisses from NE Iran.

527

528 Figure 4- SIMS U-Pb concordia and mean  $^{206}\text{Pb}/^{238}\text{U}$  age plots for the Cadomian gabbro-norites, granitic to  
529 tonalitic gneisses and metamorphosed dikes (granitic gneisses) from NE Iran.

530

531 Figure 5- A- Trace elements patterns of Cadomian upper-middle crust (felsic intrusions), middle crust  
532 (mafic intrusions) and lower crust (mafic cumulates) normalized to N-MORB. For comparison we plotted  
533 average continental crust ([Rudnick and Gao, 2003](#)), average continental delaminates ([Jagoutz and  
534 Schmidt, 2013](#)) and (NE Iran) ophiolitic cumulates ([Moghadam et al., 2014](#)). B-  $^{207}\text{Pb}/^{204}\text{Pb}$  vs  $^{206}\text{Pb}/^{204}\text{Pb}$   
535 and C-  $^{208}\text{Pb}/^{204}\text{Pb}$  vs  $^{206}\text{Pb}/^{204}\text{Pb}$  diagrams for Torud cumulate rocks. The Pb composition of pelagic  
536 sediments and continental upper and lower crust are from ([Plank and Langmuir, 1998](#)) and ([Rudnick and  
537 Gao, 2003](#)), respectively. The Pb composition of Kohistan and Famatinian arc delaminates are from  
538 ([Jagoutz and Schmidt, 2012](#)) and ([Walker et al., 2015](#)), respectively.

539

540 Figure 6- Schematic illustrations of lithological, geochronological, seismic, temperature and geochemical-  
541 isotopic evolution of the NE Iran Cadomian arc section. The calculated average continental and oceanic  
542 seismic  $V_p$  velocities and temperature are from ([Jagoutz and Behn, 2013](#)). The thickness of the individual  
543 units is approximate. Ti-in-zircon ([Watson et al., 2006](#)) and Cpx-Opx thermometry results are shown for  
544 comparison. Data for Jordanian crustal xenoliths are from ([Stern et al., 2016](#)).

545

546 Figure 7- Fractional crystallization (FC)/Assimilation-fractional crystallization (AFC) major element  
547 modelling of Cadomian magmatic rocks. Major elements have been recalculated to 100% anhydrous, in  
548 the system  $\text{SiO}_2\text{-TiO}_2\text{-Al}_2\text{O}_3\text{-FeO}^*\text{-MnO-MgO-CaO-Na}_2\text{O-K}_2\text{O}$ . *Blue* and *pink circles* represent the  
549 suspected parental melts; SH16-9 and SH16-17, respectively. *Blue* and *pink lines* represent olivine-1  
550 (O11) and olivine-2 (O12) fractionation trends respectively, as calculated for SH16-9 gabbronoritic melt.  
551 Red line represents hornblende (Hbl) fractionation trend as calculated for SH16-17 metagabbroic melt.  
552 *Green* and *orange lines* represent maximum assimilation trends as calculated for the suspected parental  
553 gabbronoritic and Hbl-metagabbroic melts, respectively. The domains of possible AFC processes are  
554 presented in *green* and *orange shaded areas* (for gabbronorite SH16-9 and metagabbro SH16-17,  
555 respectively) situated between maximum assimilation/mixing- and FC- trends.

556

557 Figure 8- La vs Yb and Nb vs Y diagrams illustrating the genesis of the Cadomian magmatic suite via FC-  
558 AFC of olivine (O11 and O12) and hornblende (Hbl) assemblages, starting from parental gabbroic samples  
559 SH16-9 and SH16-17, respectively. Bulk rock/melt partition coefficient used are reported in diagrams and  
560 were calculated following the procedure presented in section 4.4 in Appendix B. FC-curves represent, for  
561 every model, Rayleigh fractional crystallization solutions calculated for minimum  $K_D$  (min FC) and for  
562 maximum  $K_D$  (max FC) values. AFC-curves represent De Paolo Assimilation and fractional  
563 crystallization solutions. The percentages indicate amount of fractionating assemblages. Equations and  
564 parameters used are presented in Appendix B.

565

566 Figure 9- A schematic crustal column through the Cadomian arc crust of Iran. (B-E) Histograms showing  
567 the magmatic age distribution of all Cadomian rocks (B), granitoids (C), gabbros (D) and volcanic rocks  
568 (E) from Iran. (F and G) Evolution plots of isotopic (bulk rock Nd and zircon Hf) geochemistry of Iran  
569 Cadomian igneous rocks. CHUR= chondrite normalized uniform reservoir; DM= depleted mantle array  
570 (based on data from modern Mid-Oceanic Ridge basalts with  $^{176}\text{Hf}/^{177}\text{Hf}=0.28325$  and using  
571  $^{176}\text{Lu}/^{177}\text{Hf}=0.0384$  ([Chauvel and Blichert-Toft, 2001](#))). Published zircon U-Pb-Hf and bulk rock Sr-Nd  
572 data from Iran are from ([Moghadam et al., 2017b](#); [Moghadam et al., 2015](#); [Moghadam et al., 2017d](#)), data  
573 from Anatolia and Iberia are from ([Abbo et al., 2015](#); [Gursu, 2016](#); [Ustaomer et al., 2012](#)) and ([Pereira et](#)  
574 [al., 2012](#)), respectively.

575

## 576 References

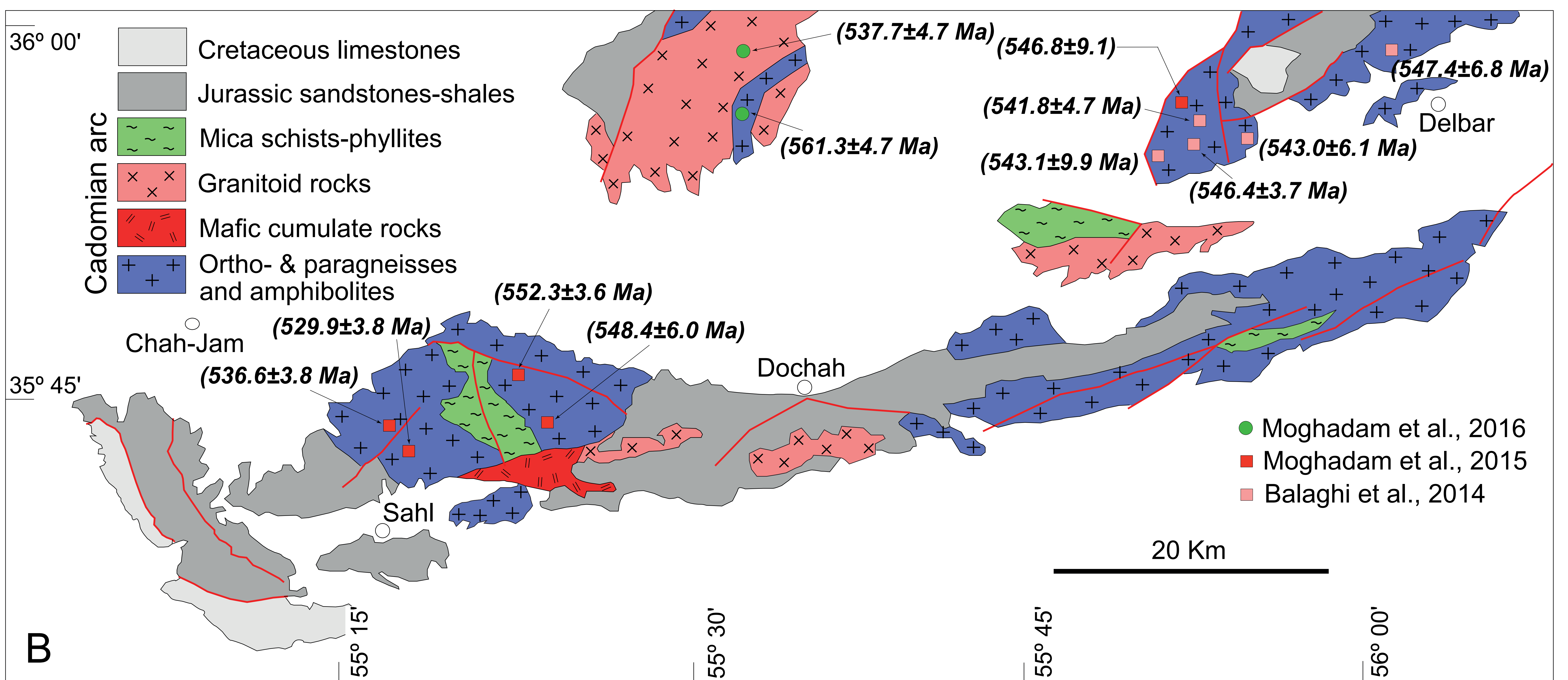
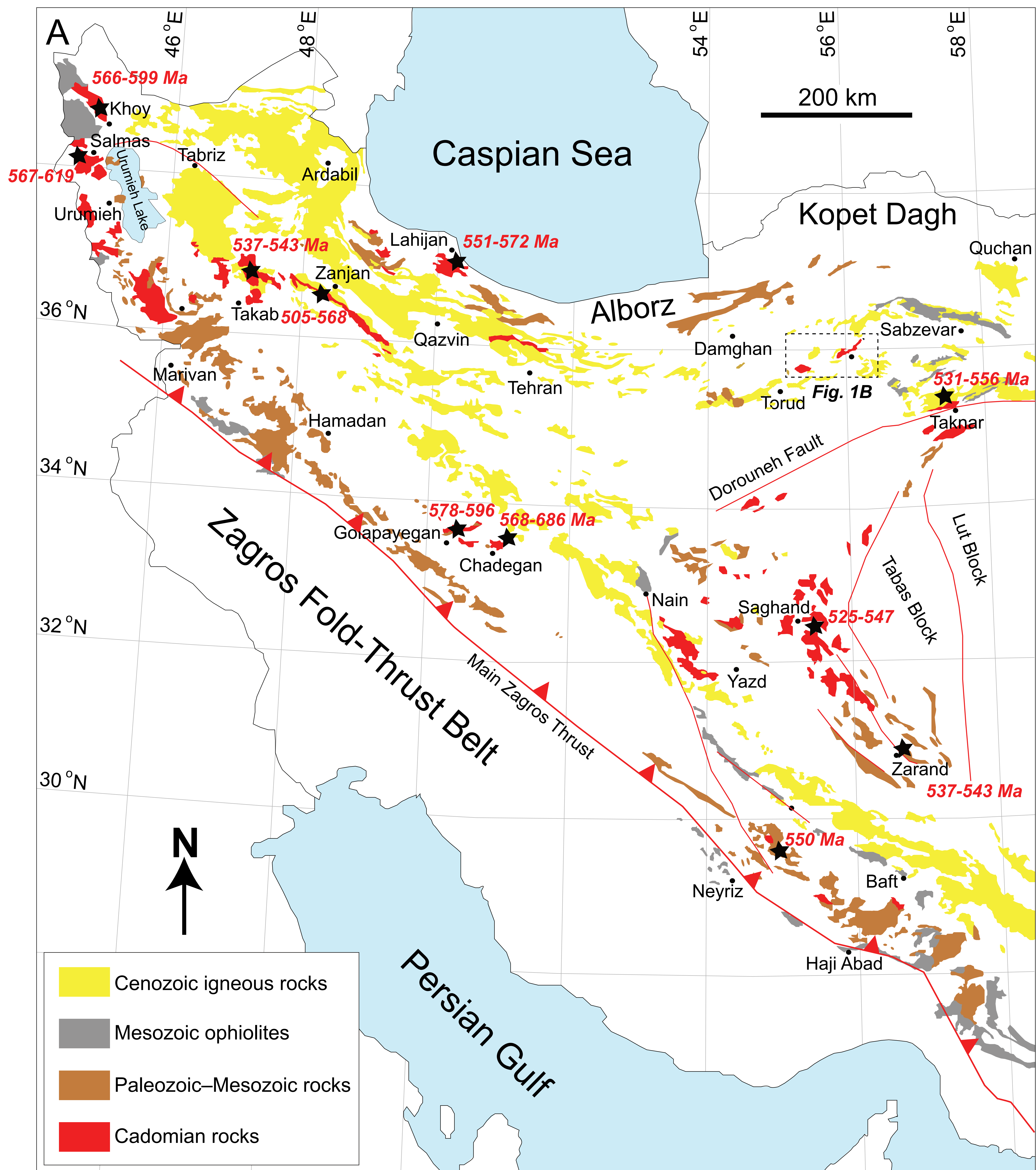
577 Abbo, A., Avigad, D., Gerdes, A., Gungor, T., 2015. Cadomian basement and Paleozoic to Triassic  
578 siliciclastics of the Taurides (Karacahisar dome, south-central Turkey): Paleogeographic constraints from  
579 U-Pb-Hf in zircons. *Lithos* 227, 122-139.

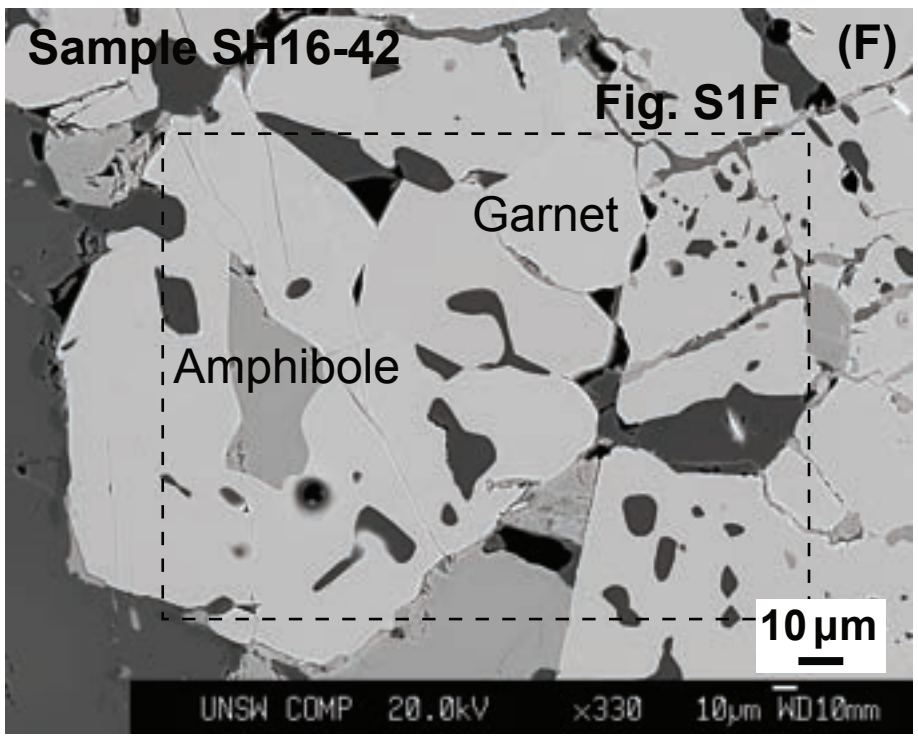
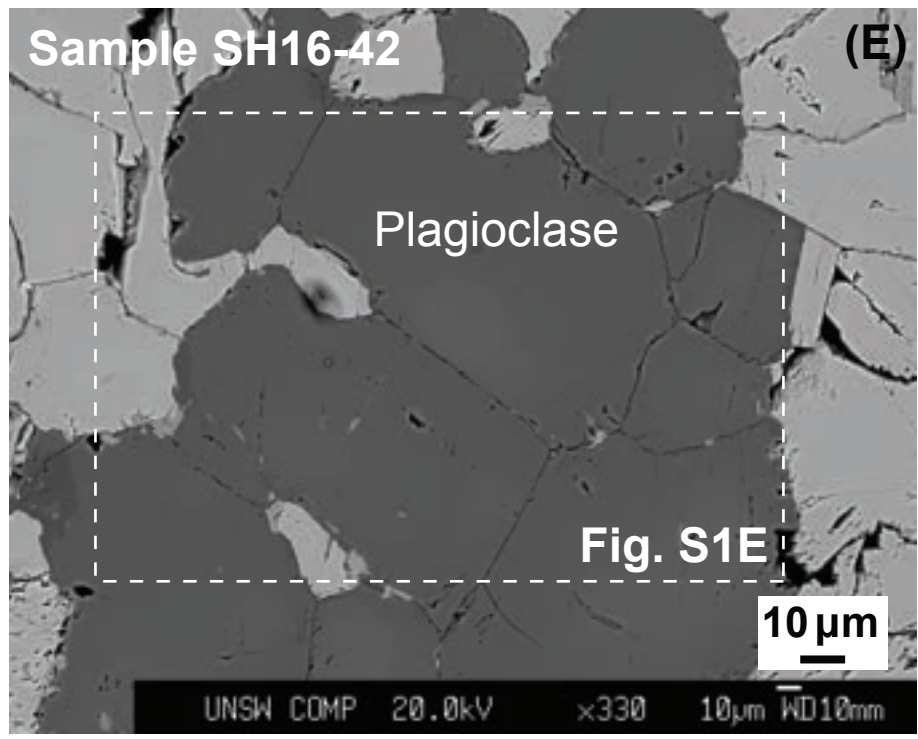
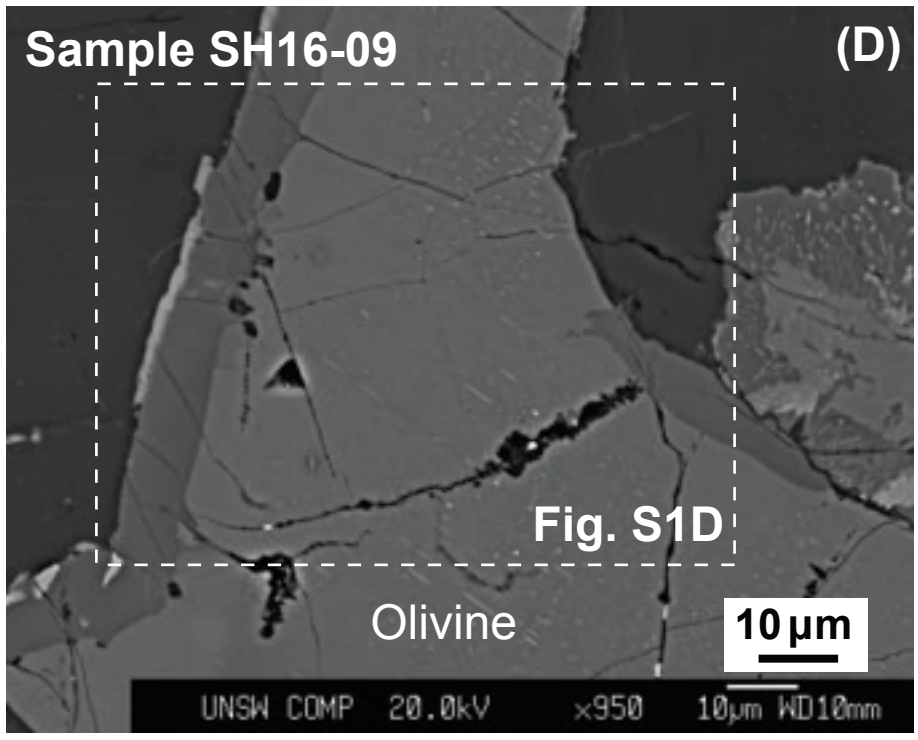
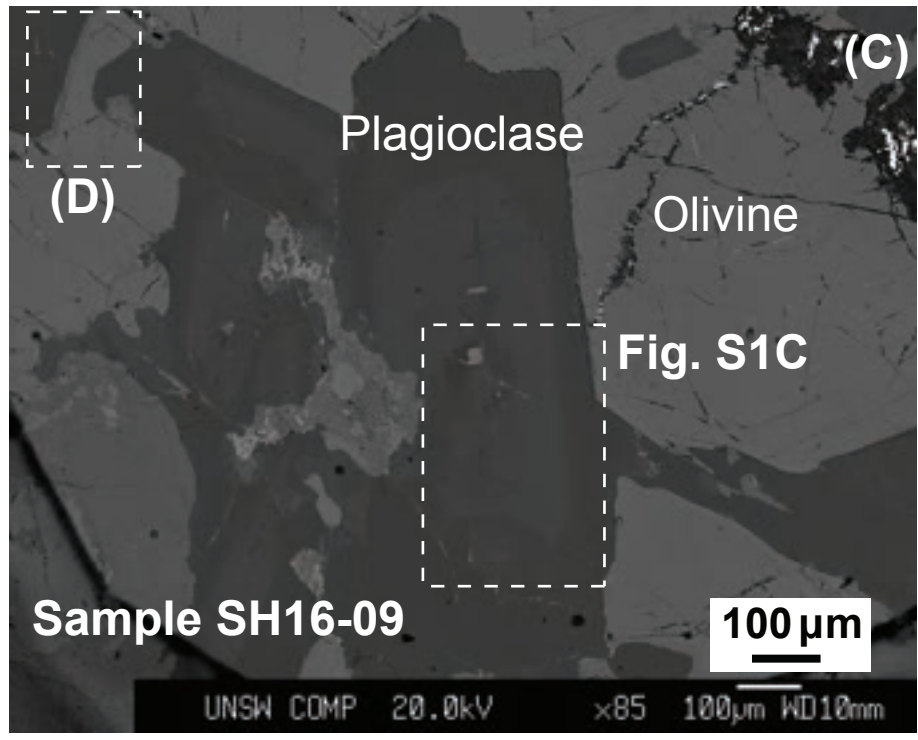
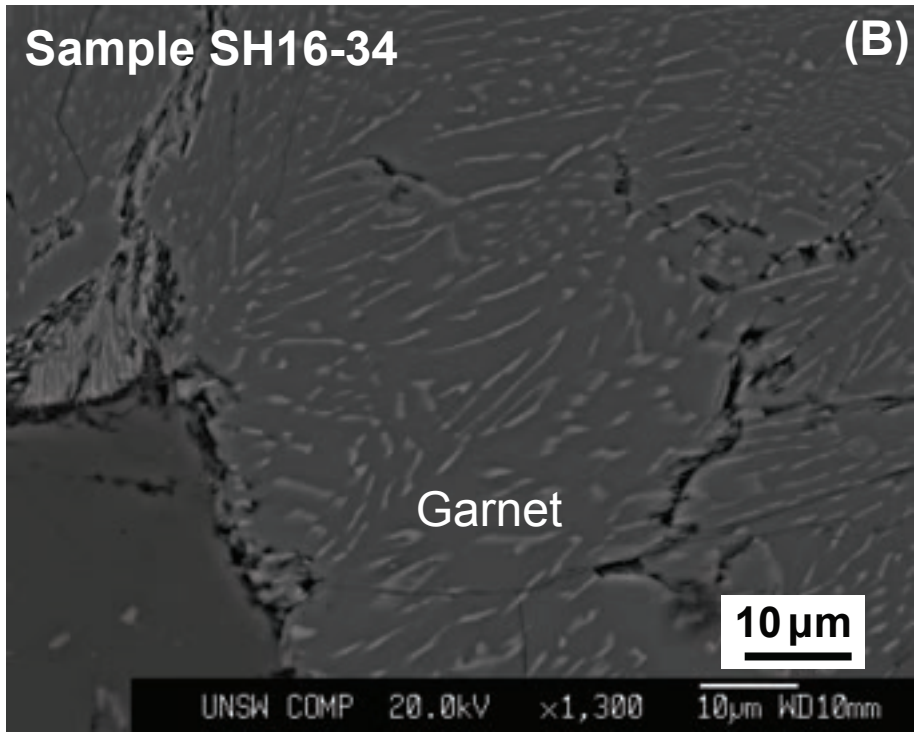
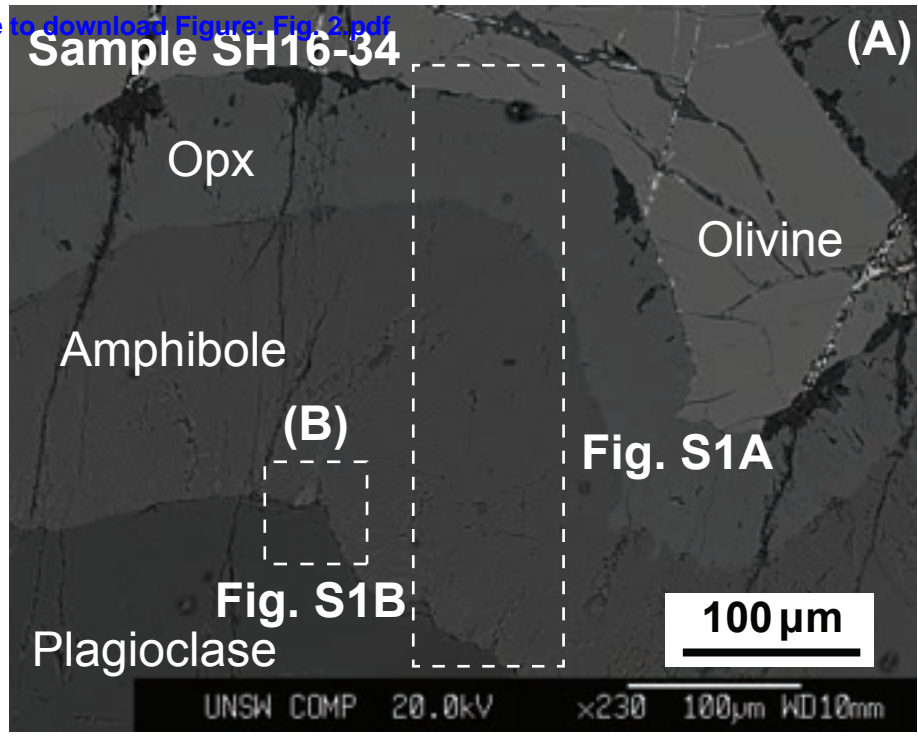
- 580 Annen, C., Blundy, J.D., Sparks, R.S.J., 2006. The genesis of intermediate and silicic magmas in deep  
581 crustal hot zones. *J Petrol* 47, 505-539.
- 582 Behn, M.D., Kelemen, P.B., 2006. Stability of arc lower crust: Insights from the Talkeetna arc section,  
583 south central Alaska, and the seismic structure of modern arcs. *Journal of Geophysical Research: Solid*  
584 *Earth* 111.
- 585 Brey, G., Köhler, T., 1990. Geothermobarometry in four-phase lherzolites II. New thermobarometers, and  
586 practical assessment of existing thermobarometers. *J Petrol* 31, 1353-1378.
- 587 Chapman, J.B., Ducea, M.N., DeCelles, P.G., Profeta, L., 2015. Tracking changes in crustal thickness  
588 during orogenic evolution with Sr/Y: An example from the North American Cordillera. *Geology* 43, 919-  
589 922.
- 590 Chapman, T., Clarke, G., Daczko, N., 2016. Crustal Differentiation in a Thickened Arc—Evaluating  
591 Depth Dependences. *J Petrol* 57, 595-620.
- 592 Chauvel, C., Blichert-Toft, J., 2001. A hafnium isotope and trace element perspective on melting of the  
593 depleted mantle. *Earth Planet Sc Lett* 190, 137-151.
- 594 Christensen, N.I., Mooney, W.D., 1995. Seismic velocity structure and composition of the continental  
595 crust: A global view. *Journal of Geophysical Research: Solid Earth* 100, 9761-9788.
- 596 DeCelles, P.G., Ducea, M.N., Kapp, P., Zandt, G., 2009. Cyclicity in Cordilleran orogenic systems. *Nat*  
597 *Geosci* 2, 251-257.
- 598 Ducea, M.N., 2002. Constraints on the bulk composition and root foundering rates of continental arcs: A  
599 California arc perspective. *J Geophys Res-Sol Ea* 107.
- 600 Ducea, M.N., Bergantz, G.W., Crowley, J.L., Otamendi, J., 2017. Ultrafast magmatic buildup and  
601 diversification to produce continental crust during subduction. *Geology* 45, 235-238.
- 602 Ducea, M.N., Paterson, S.R., DeCelles, P.G., 2015a. High-Volume Magmatic Events in Subduction  
603 Systems. *Elements* 11, 99-104.
- 604 Ducea, M.N., Saleeby, J.B., Bergantz, G., 2015b. The Architecture, Chemistry, and Evolution of  
605 Continental Magmatic Arcs. *Annual Review of Earth and Planetary Sciences*, Vol 43 43, 299-331.
- 606 Gursu, S., 2016. A new petrogenetic model for meta-granitic rocks in the central and southern Menderes  
607 Massif - W Turkey: Implications for Cadomian crustal evolution within the Pan-African mega-cycle.  
608 *Precambrian Res* 275, 450-470.
- 609 Hammarstrom, J.M., Zen, E.-a., 1986. Aluminum in hornblende: an empirical igneous geobarometer. *Am*  
610 *Mineral* 71, 1297-1313.
- 611 Hosseini, S.H., Sadeghian, M., Zhai, M.G., Ghasemi, H., 2015. Petrology, geochemistry and zircon U-Pb  
612 dating of Band-e-Hezarchah metabasites (NE Iran): An evidence for back-arc magmatism along the  
613 northern active margin of Gondwana. *Chem Erde-Geochem* 75, 207-218.
- 614 Jagoutz, O., 2014. Arc crustal differentiation mechanisms. *Earth Planet Sc Lett* 396, 267-277.

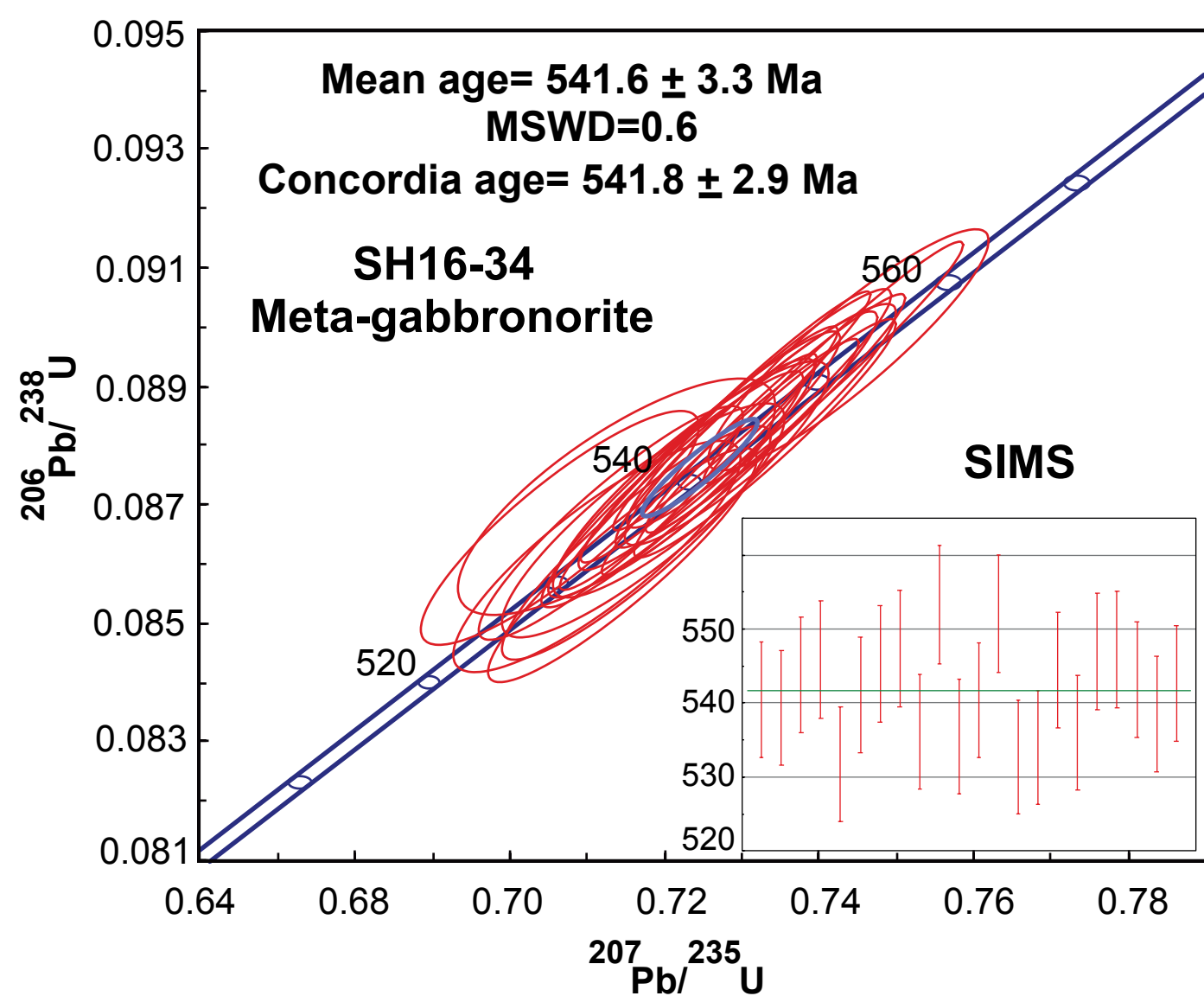
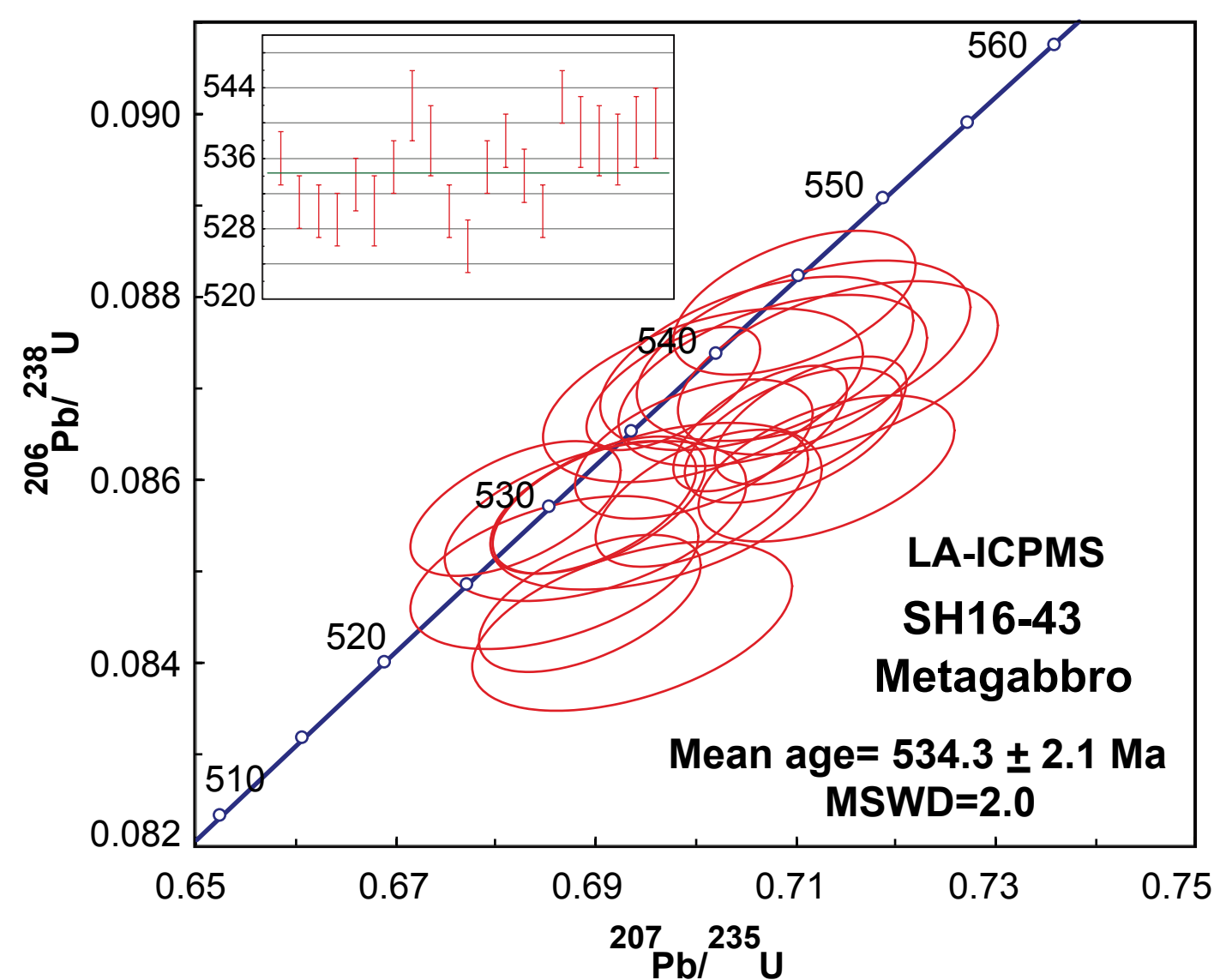
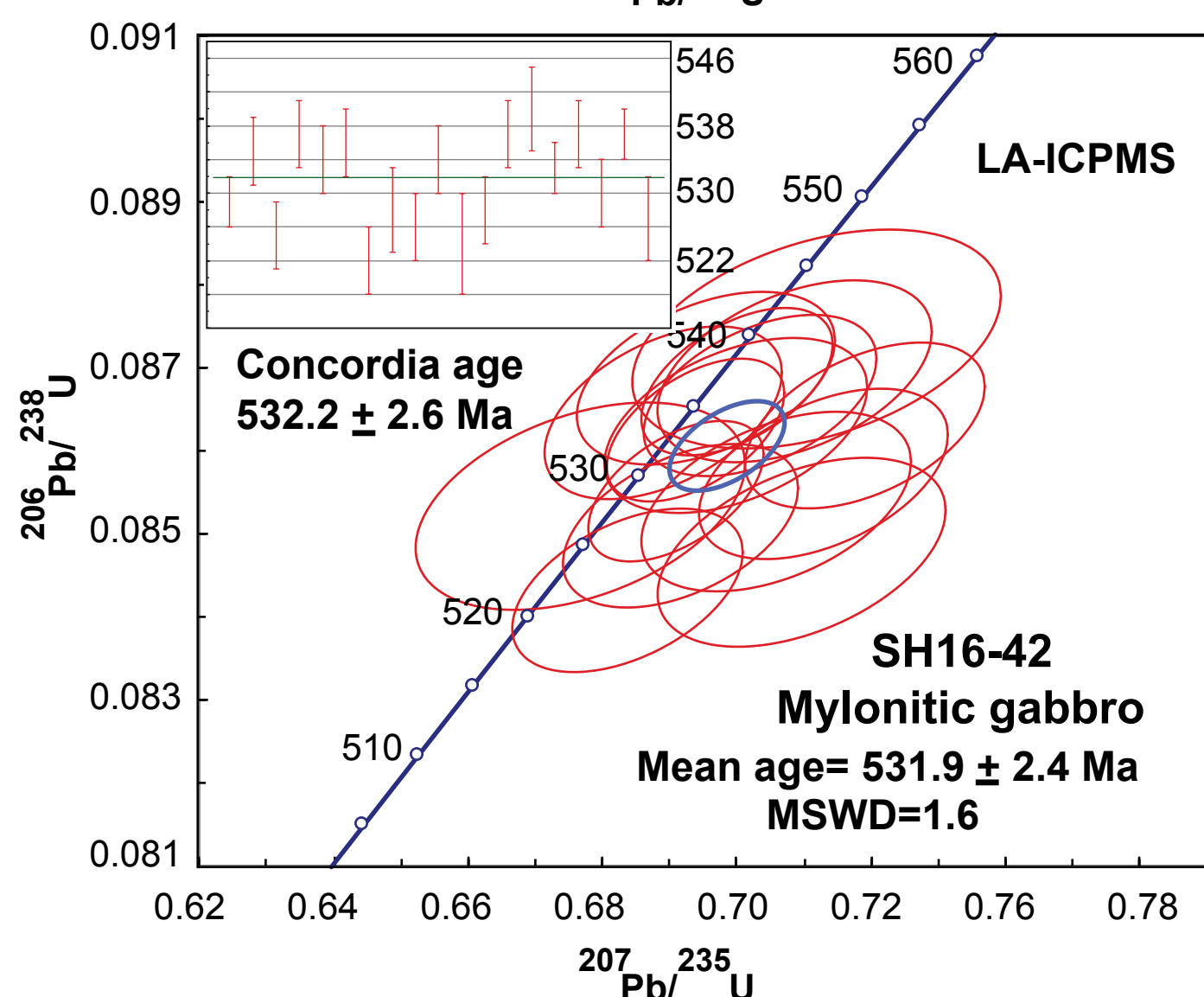
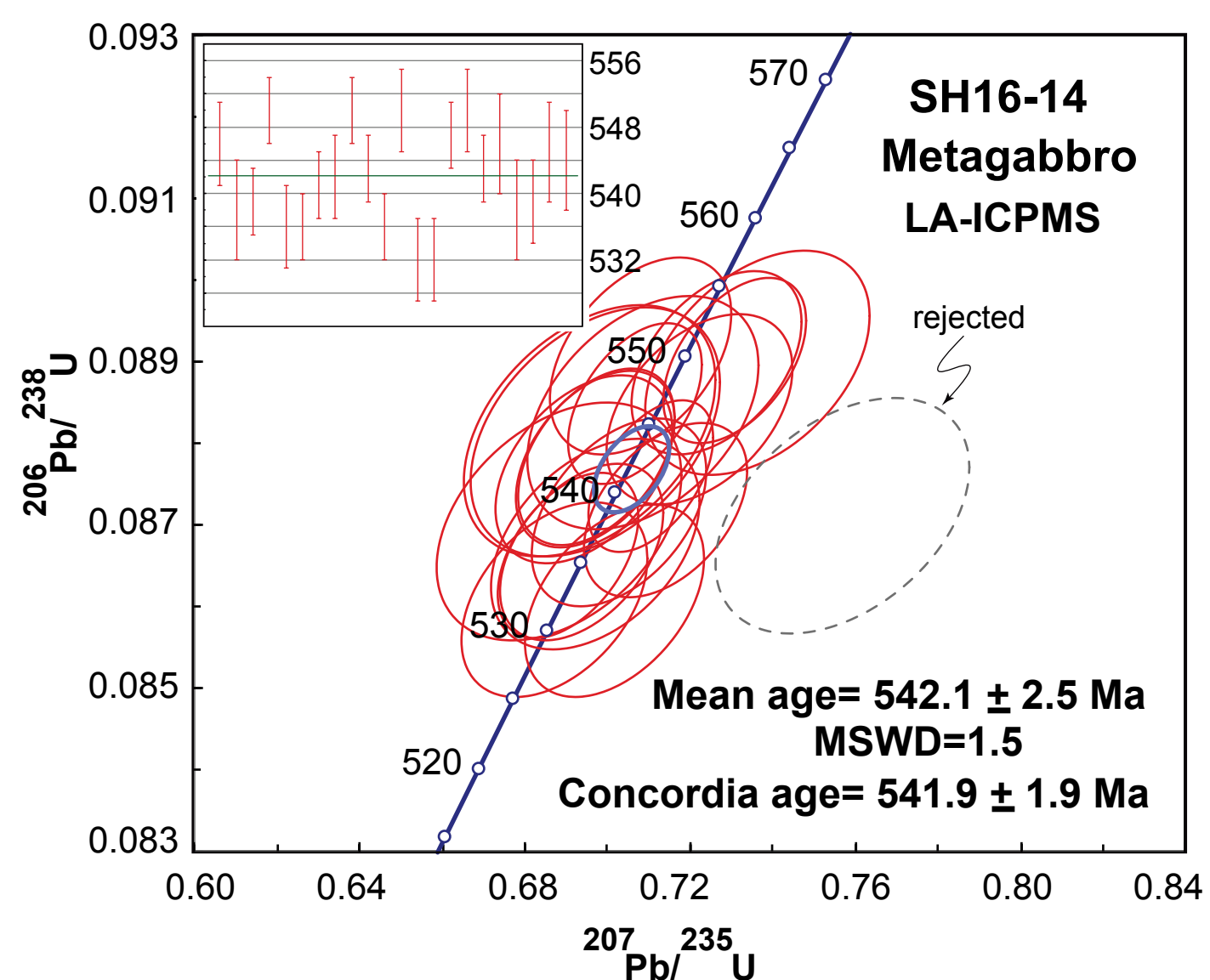
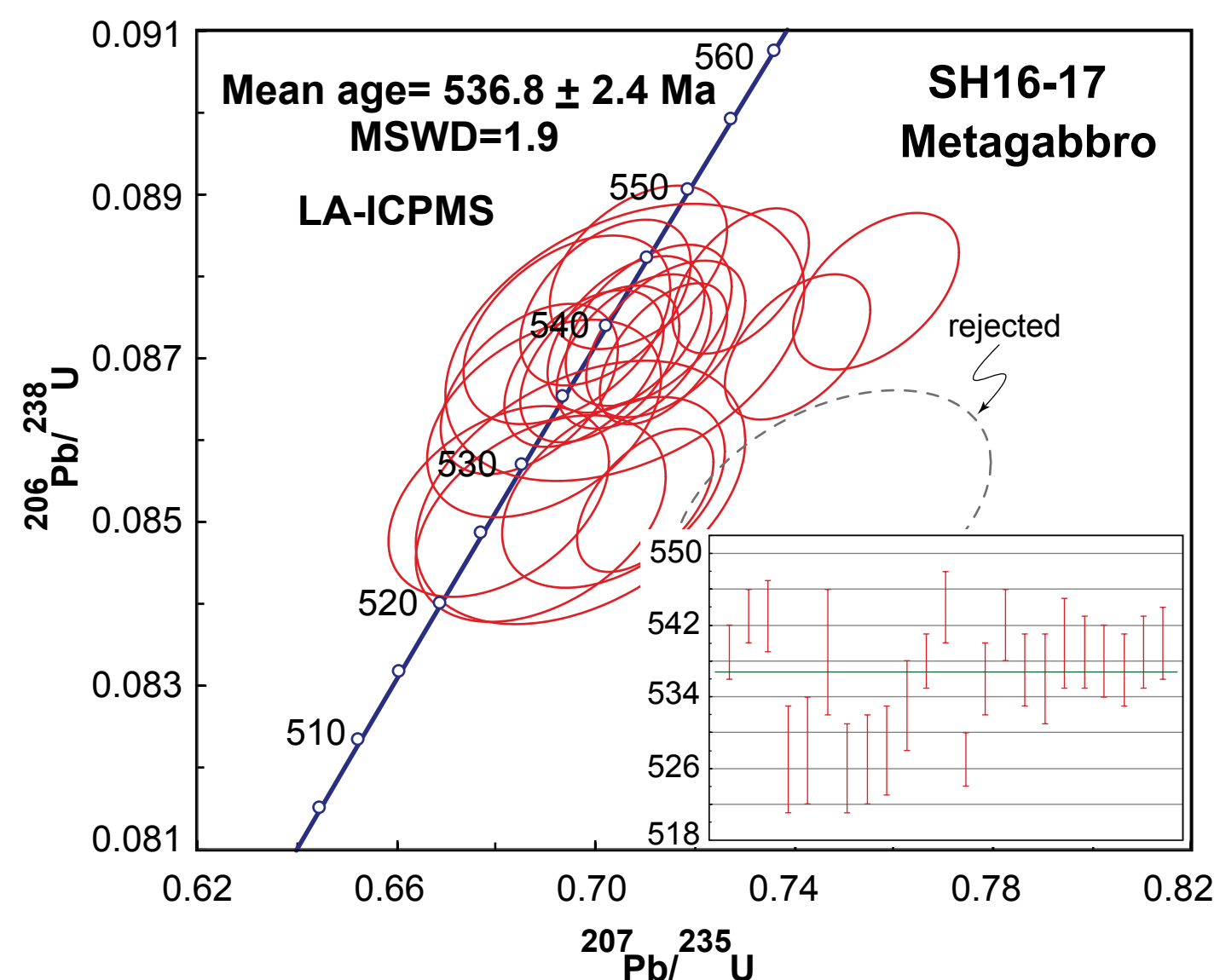
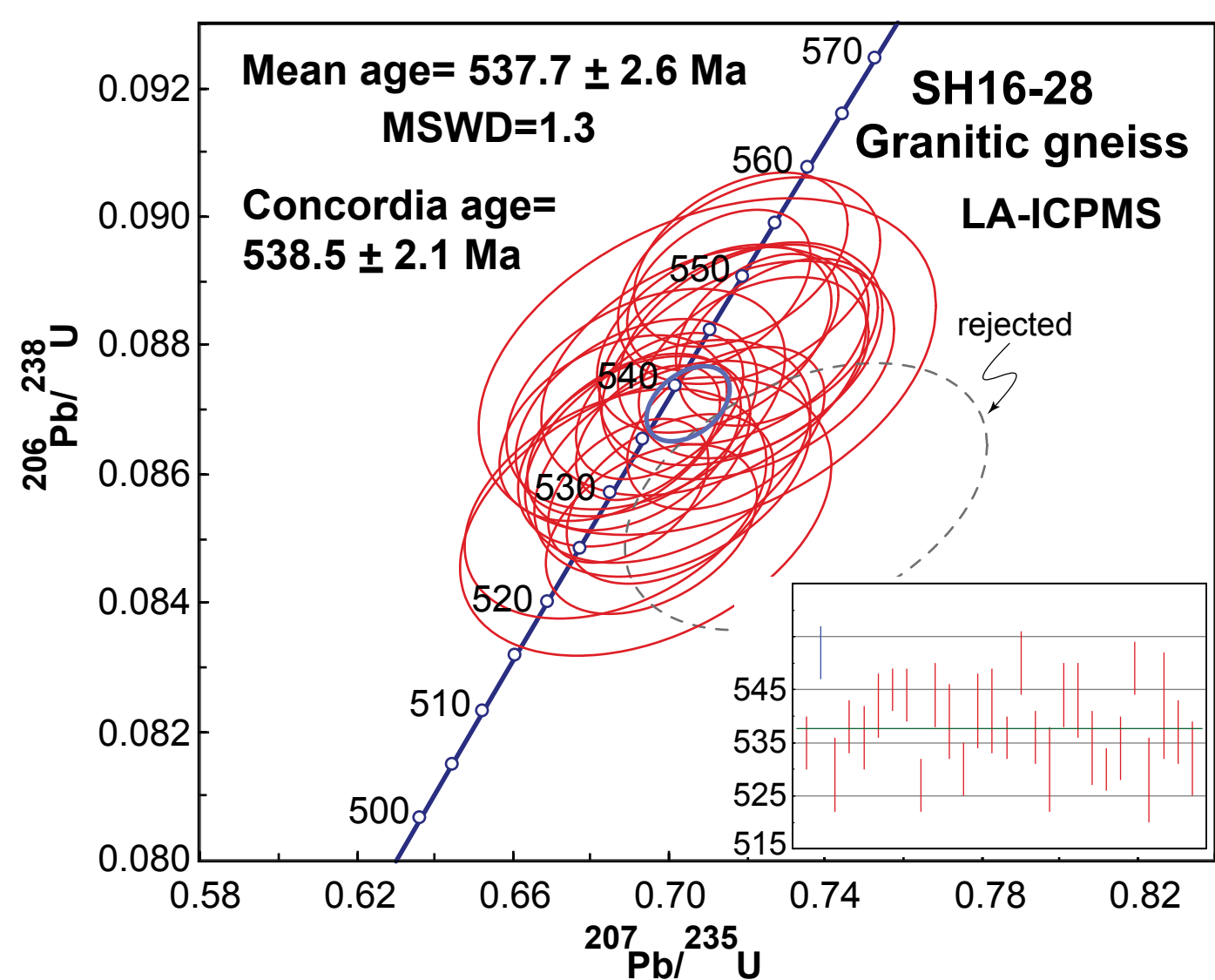
- 615 Jagoutz, O., Behn, M.D., 2013. Foundering of lower island-arc crust as an explanation for the origin of  
616 the continental Moho. *Nature* 504, 131.
- 617 Jagoutz, O., Schmidt, M., 2013. The composition of the foundered complement to the continental crust  
618 and a re-evaluation of fluxes in arcs. *Earth Planet Sc Lett* 371, 177-190.
- 619 Jagoutz, O., Schmidt, M.W., 2012. The formation and bulk composition of modern juvenile continental  
620 crust: The Kohistan arc. *Chem Geol* 298, 79-96.
- 621 Jicha, B.R., Jagoutz, O., 2015. Magma Production Rates for Intraoceanic Arcs. *Elements* 11, 105-111.
- 622 Kitamura, K., Ishikawa, M., Arima, M., 2003. Petrological model of the northern Izu-Bonin-Mariana arc  
623 crust: constraints from high-pressure measurements of elastic wave velocities of the Tanzawa plutonic  
624 rocks, central Japan. *Tectonophysics* 371, 213-221.
- 625 Lackey, J.S., Valley, J.W., Saleeby, J.B., 2005. Supracrustal input to magmas in the deep crust of Sierra  
626 Nevada batholith: Evidence from high-delta O-18 zircon. *Earth Planet Sc Lett* 235, 315-330.
- 627 Linnemann, U., Romer, R.L., Gerdes, A., Jeffries, T.E., Drost, K., Ulrich, J., 2010. The Cadomian  
628 Orogeny in the Saxo-Thuringian Zone, in: Linnemann, U., Romer, R.L. (Eds.), *Pre-Mesozoic Geology of*  
629 *Saxo-Thuringia – From the Cadomian Active Margin to the Variscan Orogen*, Schweizerbart, Stuttgart,  
630 pp. 37-58.
- 631 Malekpour-Alamdari, A., Axen, G., Heizler, M., Hassanzadeh, J., 2017. Large-magnitude continental  
632 extension in the northeastern Iranian Plateau: Insight from K-feldspar  $^{40}\text{Ar}/^{39}\text{Ar}$  thermochronology from  
633 the Shotor Kuh-Biarjmand metamorphic core complex. *Geosphere* 13, 1207-1233.
- 634 Mantle, G., Collins, W., 2008. Quantifying crustal thickness variations in evolving orogens: Correlation  
635 between arc basalt composition and Moho depth. *Geology* 36, 87-90.
- 636 McBirney, A., Taylor, H., Armstrong, R., 1987. Paricutin re-examined: a classic example of crustal  
637 assimilation in calc-alkaline magma. *Contrib Mineral Petr* 95, 4-20.
- 638 Moghadam, H.S., Bröcker, M., Griffin, W.L., Li, X.H., Chen, R.X., O'Reilly, S.Y., 2017a. Subduction,  
639 high-P metamorphism, and collision fingerprints in South Iran: Constraints from zircon U-Pb and mica  
640 Rb-Sr geochronology. *Geochemistry, Geophysics, Geosystems* 18, 306-332.
- 641 Moghadam, H.S., Corfu, F., Chiaradia, M., Stern, R.J., Ghorbani, G., 2014. Sabzevar Ophiolite, NE Iran:  
642 Progress from embryonic oceanic lithosphere into magmatic arc constrained by new isotopic and  
643 geochemical data. *Lithos* 210, 224-241.
- 644 Moghadam, H.S., Griffin, W.L., Li, X.H., Santos, J.F., Karsli, O., Stern, R.J., Ghorbani, G., Gain, S.,  
645 Murphy, R., O'Reilly, S.Y., 2017b. Crustal Evolution of NW Iran: Cadomian Arcs, Archean Fragments  
646 and the Cenozoic Magmatic Flare-Up. *J Petrol* 58, 2143-2190.
- 647 Moghadam, H.S., Khademi, M., Hu, Z.C., Stern, R.J., Santos, J.F., Wu, Y.B., 2015. Cadomian  
648 (Ediacaran-Cambrian) arc magmatism in the ChahJam-Biarjmand metamorphic complex (Iran):  
649 Magmatism along the northern active margin of Gondwana. *Gondwana Res* 27, 439-452.

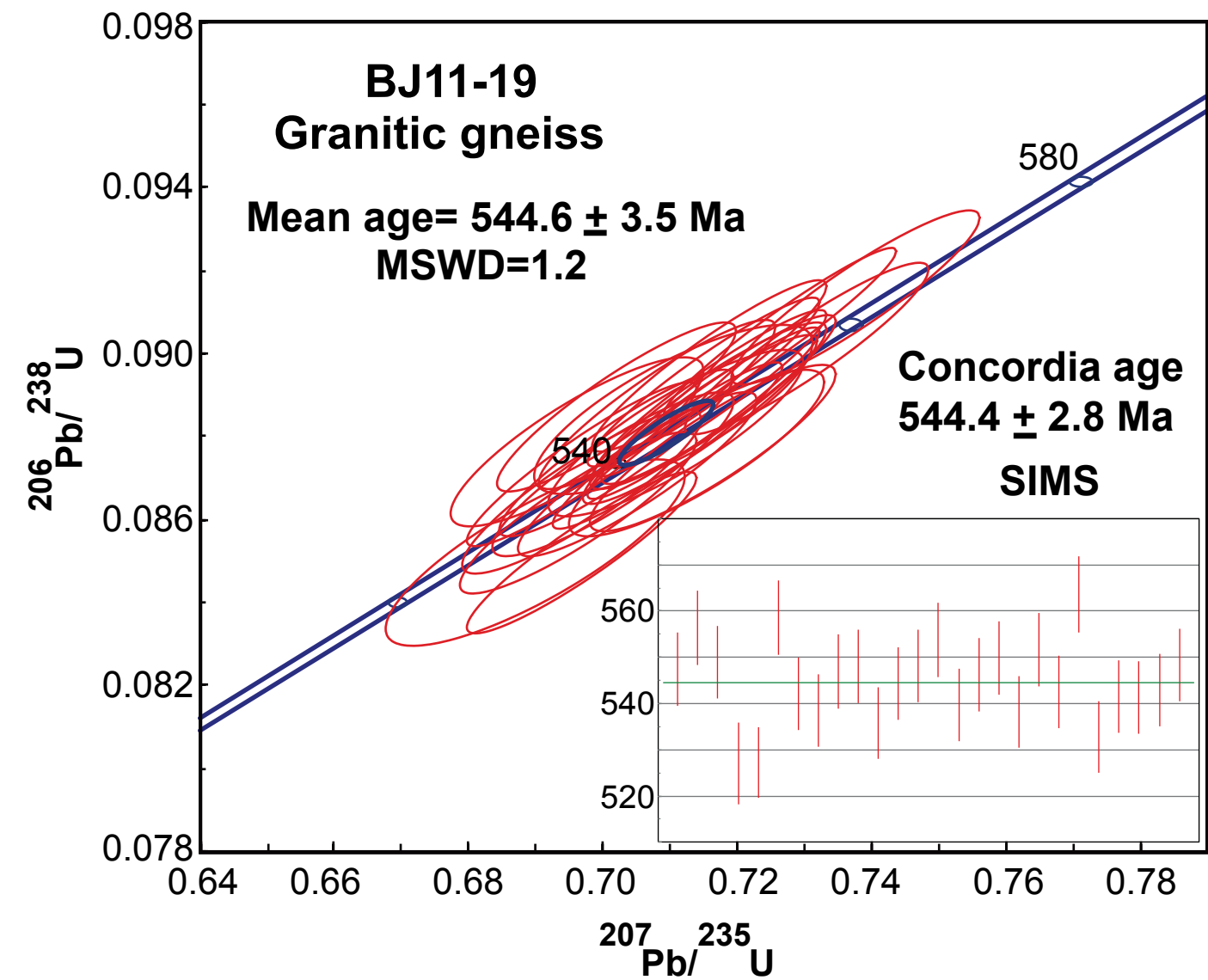
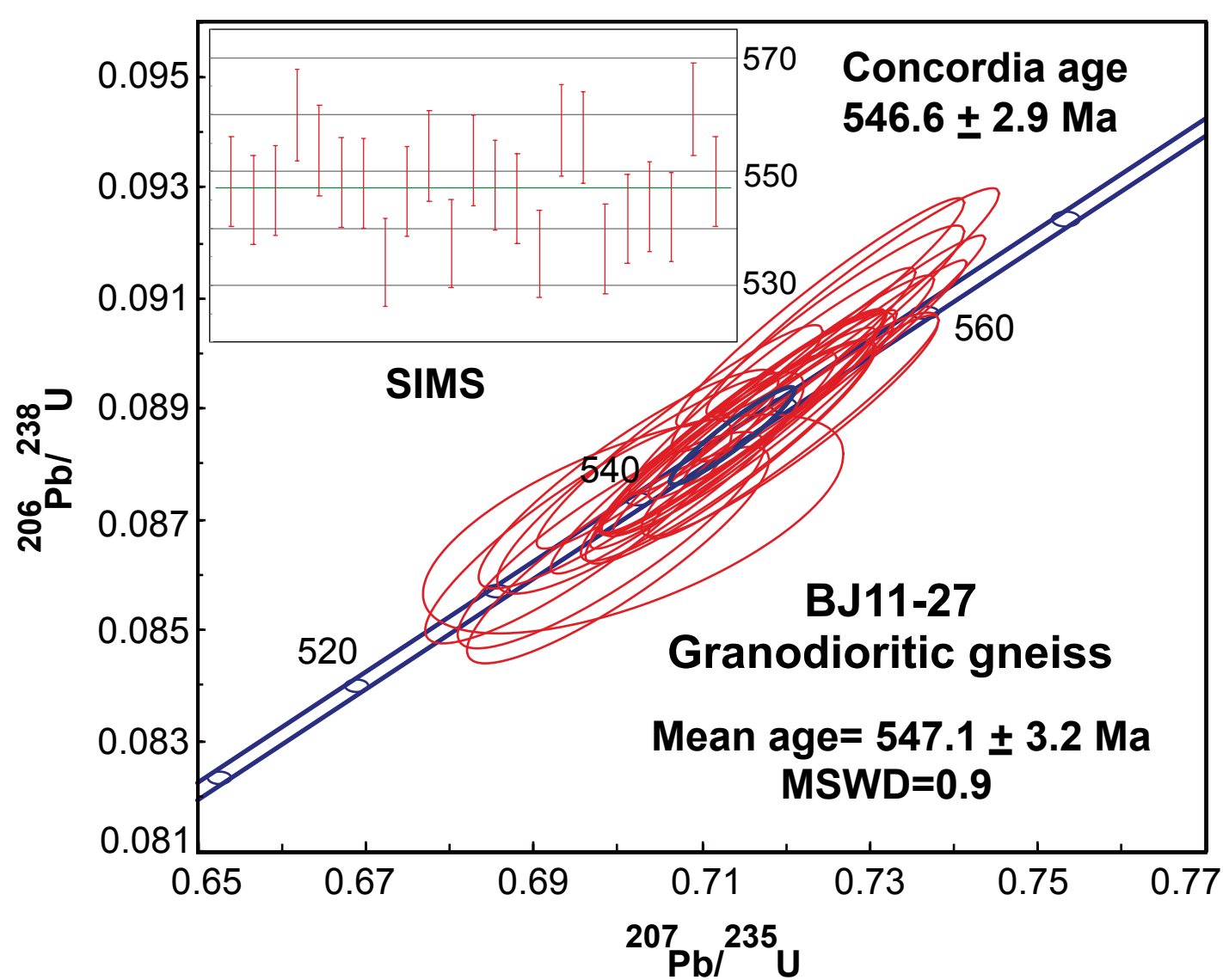
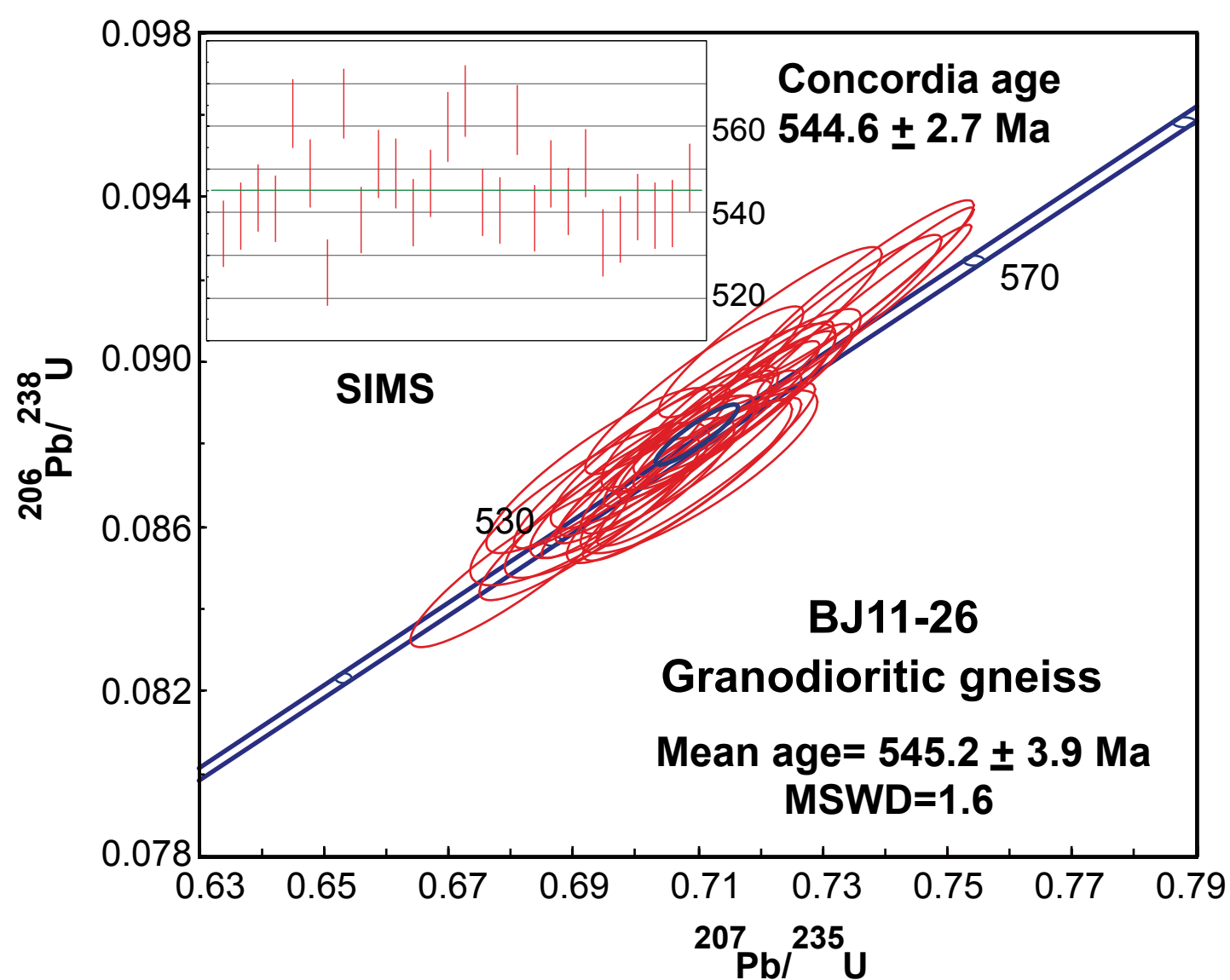
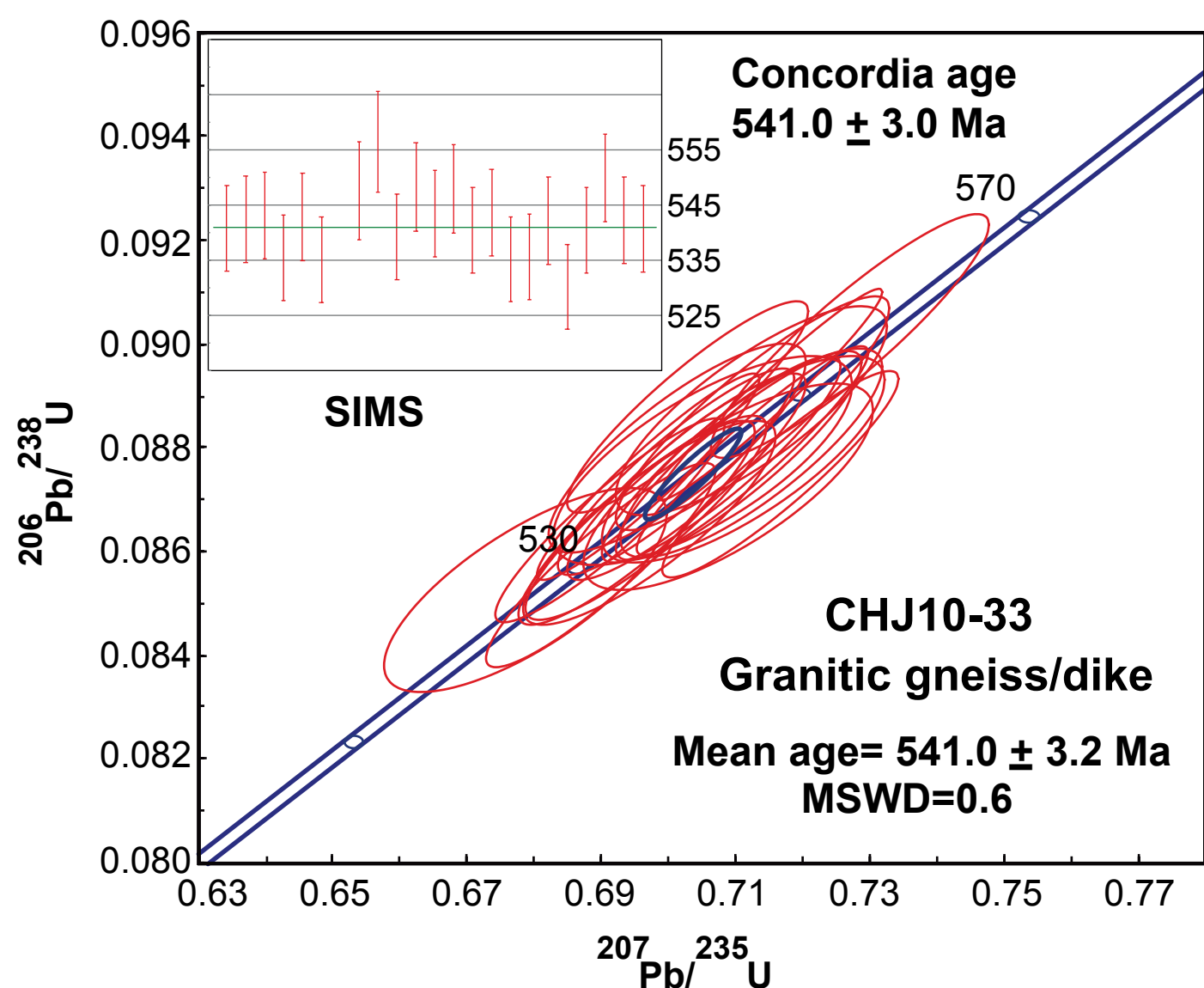
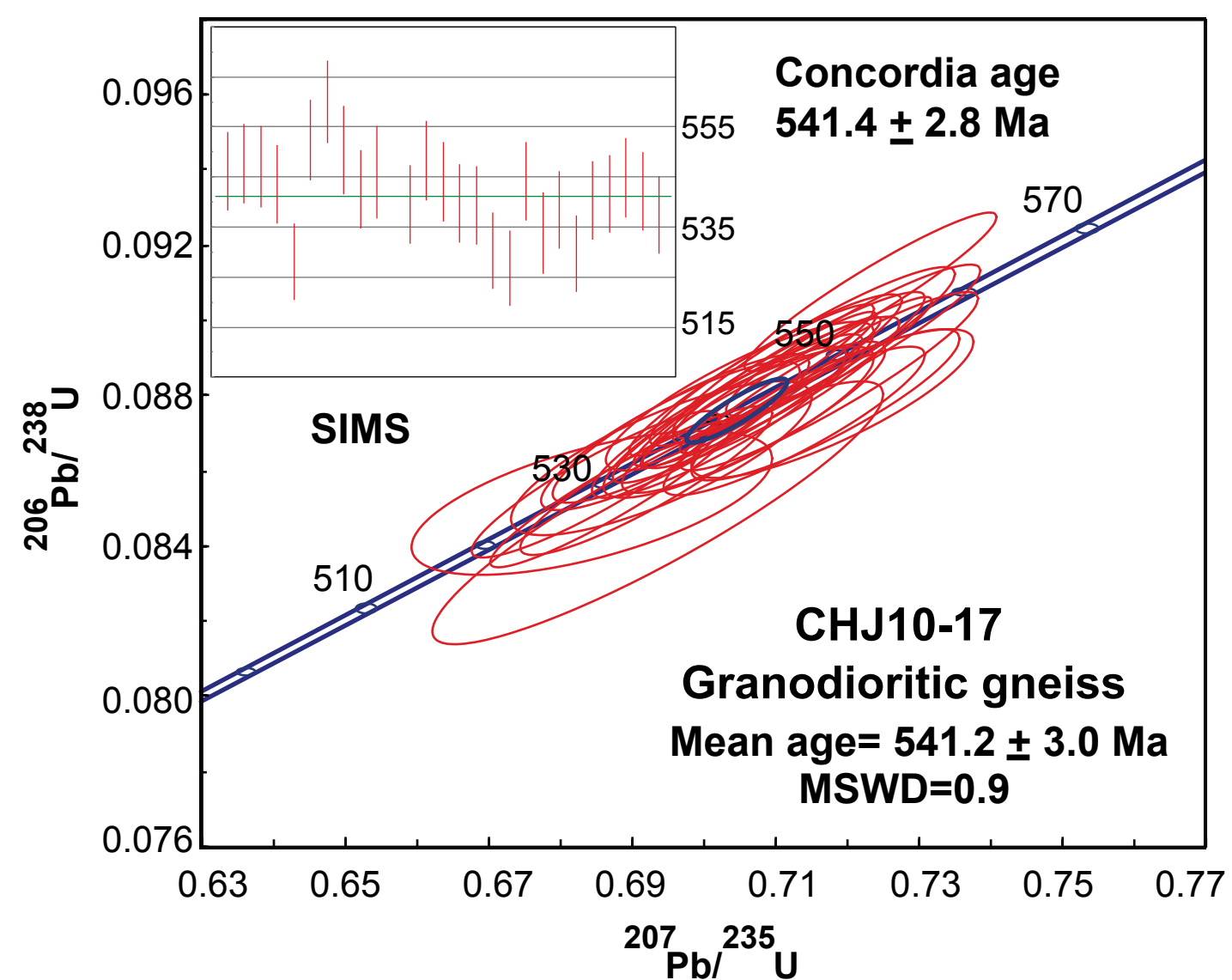
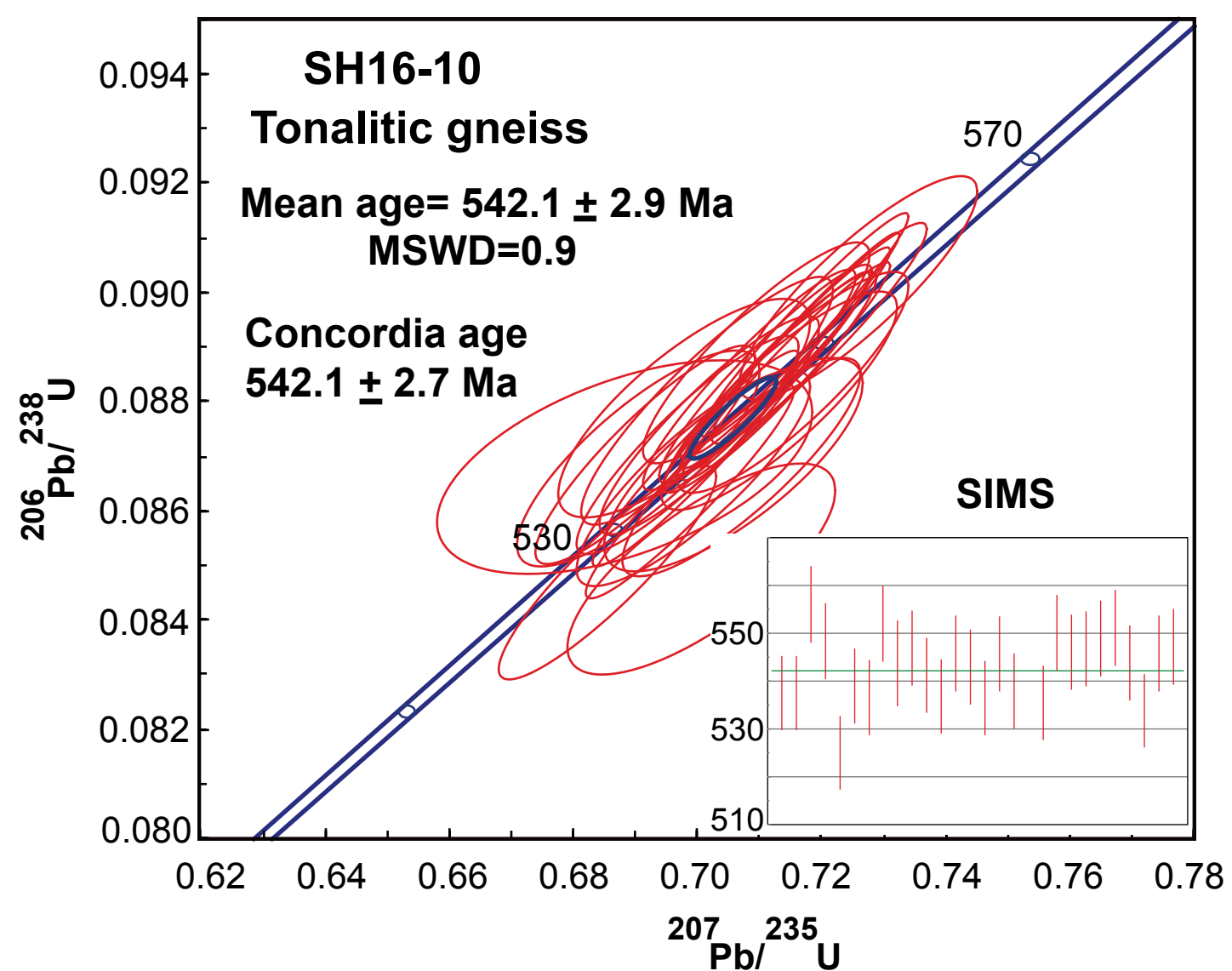
- 650 Moghadam, H.S., Li, X.-H., Griffin, W.L., Stern, R.J., Thomsen, T.B., Meinhold, G., Aharipour, R.,  
651 O'Reilly, S.Y., 2017c. Early Paleozoic tectonic reconstruction of Iran: Tales from detrital zircon  
652 geochronology. *Lithos* 268, 87-101.
- 653 Moghadam, H.S., Li, X.-H., Santos, J.F., Stern, R.J., Griffin, W.L., Ghorbani, G., Sarebani, N., 2017d.  
654 Neoproterozoic magmatic flare-up along the N. margin of Gondwana: The Taknar complex, NE Iran.  
655 *Earth Planet Sc Lett* 474, 83-96.
- 656 Muntener, O., Kelemen, P.B., Grove, T.L., 2001. The role of H<sub>2</sub>O during crystallization of primitive arc  
657 magmas under uppermost mantle conditions and genesis of igneous pyroxenites: an experimental study.  
658 *Contrib Mineral Petr* 141, 643-658.
- 659 Otamendi, J.E., Pinotti, L.P., Basei, M.A.S., Tibaldi, A.M., 2010. Evaluation of petrogenetic models for  
660 intermediate and silicic plutonic rocks from the Sierra de Valle Fertil-La Huerta, Argentina: Petrologic  
661 constraints on the origin of igneous rocks in the Ordovician Famatinian-Puna paleoarc. *J S Am Earth Sci*  
662 30, 29-45.
- 663 Paterson, S.R., Ducea, M.N., 2015. Arc Magmatic Tempos: Gathering the Evidence. *Elements* 11, 91-97.
- 664 Pereira, M.F., Sola, A.R., Chichorro, M., Lopes, L., Gerdes, A., Silva, J.B., 2012. North-Gondwana  
665 assembly, break-up and paleogeography: U-Pb isotope evidence from detrital and igneous zircons of  
666 Ediacaran and Cambrian rocks of SW Iberia. *Gondwana Res* 22, 866-881.
- 667 Plank, T., Langmuir, C.H., 1998. The chemical composition of subducting sediment and its consequences  
668 for the crust and mantle. *Chem Geol* 145, 325-394.
- 669 Rahmati-Ilkhchi, M., Jerabek, P., Faryad, S.W., Koyi, H.A., 2010. Mid-Cimmerian, Early Alpine and  
670 Late Cenozoic orogenic events in the Shotur Kuh metamorphic complex, Great Kavir block, NE Iran.  
671 *Tectonophysics* 494, 101-117.
- 672 Rudnick, R., Gao, S., 2003. Composition of the continental crust. *Treatise on geochemistry* 3, 659.
- 673 Schmidt, M.W., 1992. Amphibole composition in tonalite as a function of pressure: an experimental  
674 calibration of the Al-in-hornblende barometer. *Contrib Mineral Petr* 110, 304-310.
- 675 Stern, R.J., Ali, K.A., Ren, M., Jarrar, G.H., Romer, R.L., Leybourne, M.I., Whitehouse, M.J., Ibrahim,  
676 K.M., 2016. Cadomian (~ 560 Ma) crust buried beneath the northern Arabian Peninsula: Mineral,  
677 chemical, geochronological, and isotopic constraints from NE Jordan xenoliths. *Earth Planet Sc Lett* 436,  
678 31-42.
- 679 Stern, R.J., Tamura, Y., Ishizuka, O., Shukano, H., Bloomer, S.H., Embley, R.W., Leybourne, M.,  
680 Kawabata, H., Nunokawa, A., Nichols, A.R., 2014. Volcanoes of the Diamante cross-chain: evidence for  
681 a mid-crustal felsic magma body beneath the Southern Izu–Bonin–Mariana arc. *Geological Society,*  
682 *London, Special Publications* 385, 235-255.
- 683 Stern, R.J., Tamura, Y., Shukuno, H., Miyazaki, T., 2019. The Zealandia Volcanic Complex: Further  
684 evidence of a lower crustal “hot zone” beneath the Mariana Intra-oceanic Arc, Western Pacific. *Isl Arc*.
- 685 Stuart, C., Daczko, N., Piazzolo, S., 2016. Local partial melting of the lower crust triggered by hydration  
686 through melt–rock interaction: an example from Fiordland, New Zealand. *J Metamorph Geol*.

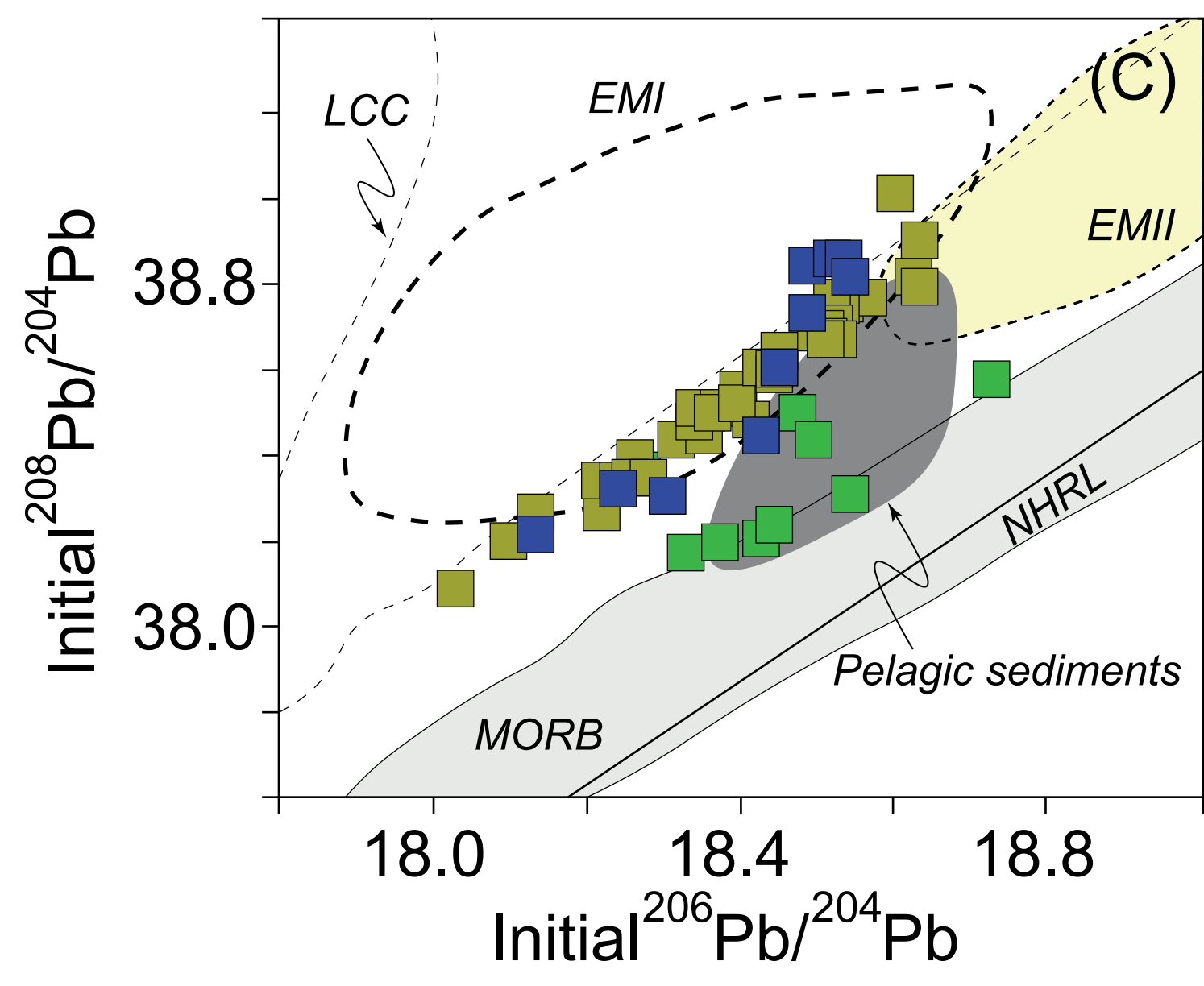
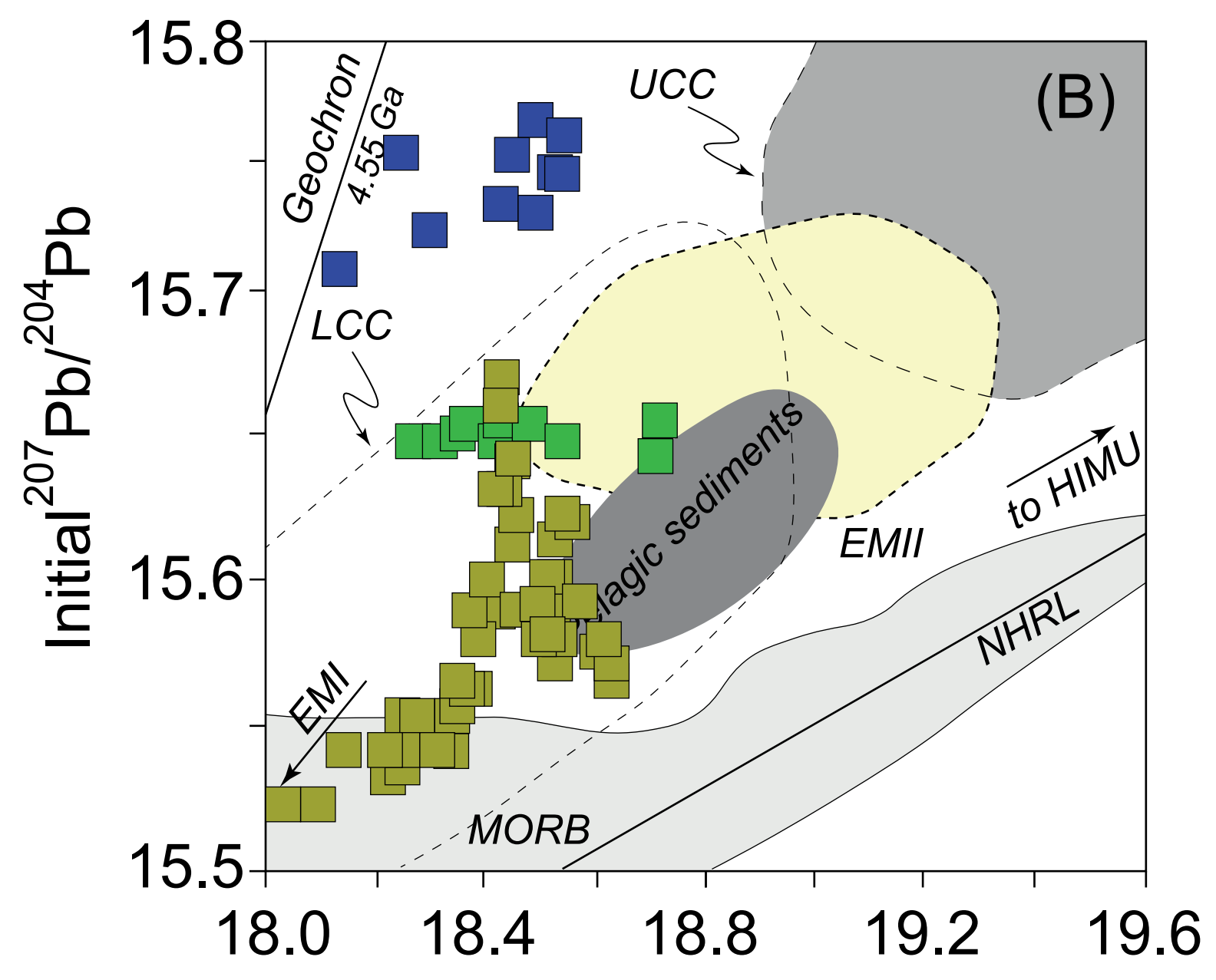
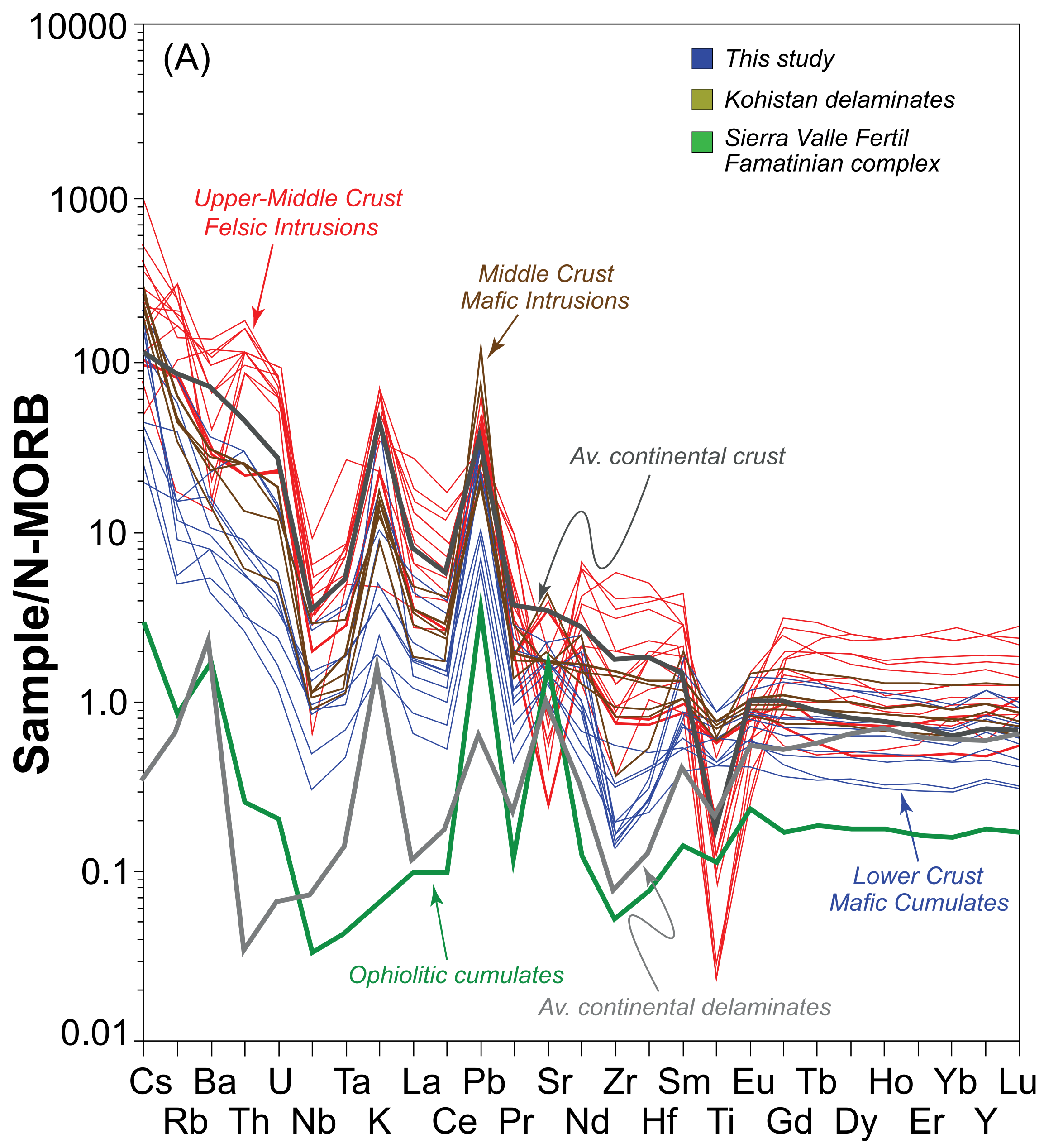
- 687 Tilhac, R., Ceuleneer, G., Griffin, W.L., O'Reilly, S.Y., Pearson, N.J., Benoit, M., Henry, H., Girardeau,  
688 J., Grégoire, M., 2016. Primitive Arc Magmatism and Delamination: Petrology and Geochemistry of  
689 Pyroxenites from the Cabo Ortegal Complex, Spain. *J Petrol* 57, 1921-1954.
- 690 Ustaomer, P.A., Ustaomer, T., Gerdes, A., Robertson, A.H.F., Collins, A.S., 2012. Evidence of  
691 Precambrian sedimentation/magmatism and Cambrian metamorphism in the Bitlis Massif, SE Turkey  
692 utilising whole-rock geochemistry and U-Pb LA-ICP-MS zircon dating. *Gondwana Res* 21, 1001-1018.
- 693 Verdel, C., Wernicke, B.P., Ramezani, J., Hassanzadeh, J., Renne, P.R., Spell, T.L., 2007. Geology and  
694 thermochronology of Tertiary Cordilleran-style metamorphic core complexes in the Saghand region of  
695 central Iran. *Geol Soc Am Bull* 119, 961-977.
- 696 Walker, B.A., Bergantz, G.W., Otamendi, J.E., Ducea, M.N., Cristofolini, E.A., 2015. A MASH Zone  
697 Revealed: the Mafic Complex of the Sierra Valle Fertil. *J Petrol* 56, 1863-1896.
- 698 Watson, E.B., Wark, D.A., Thomas, J.B., 2006. Crystallization thermometers for zircon and rutile.  
699 *Contrib Mineral Petr* 151, 413-433.  
700

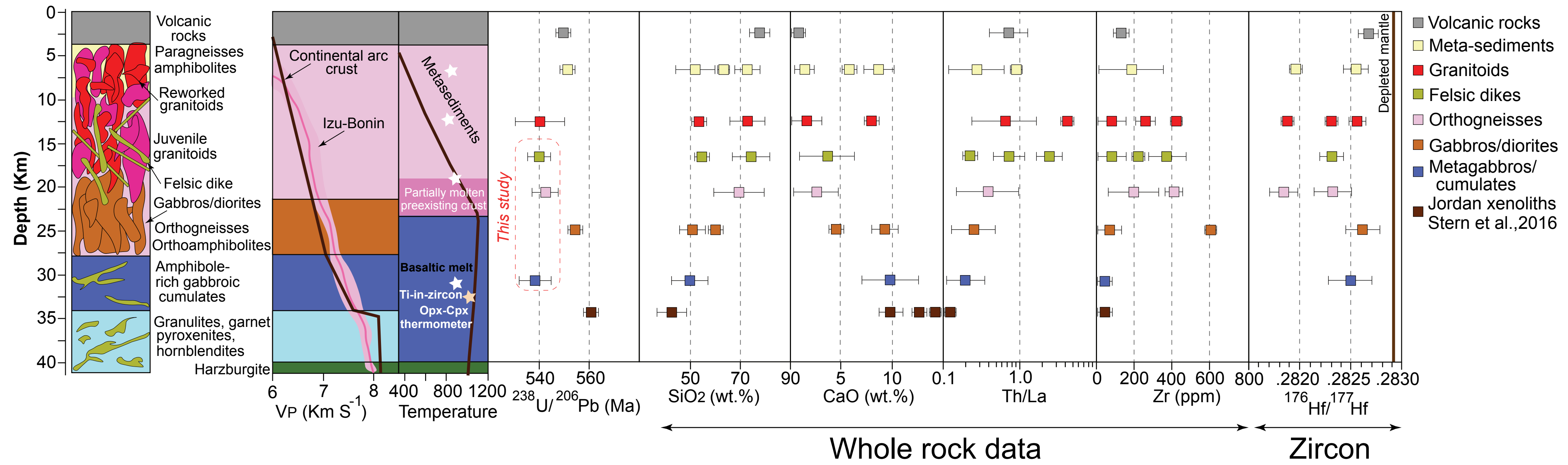


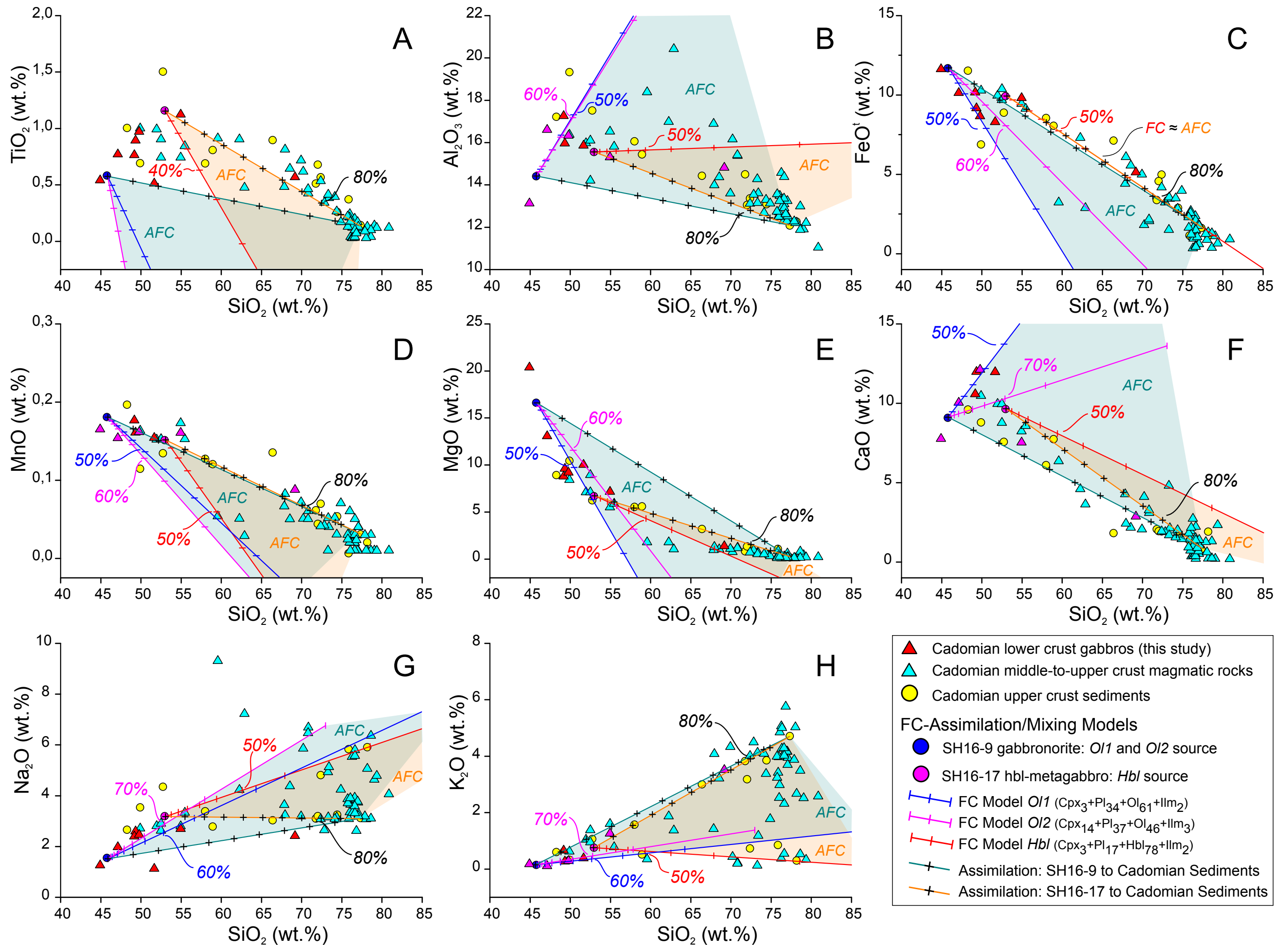


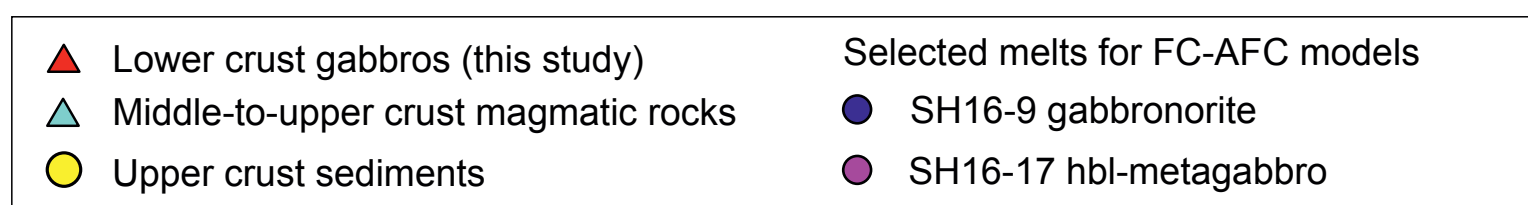
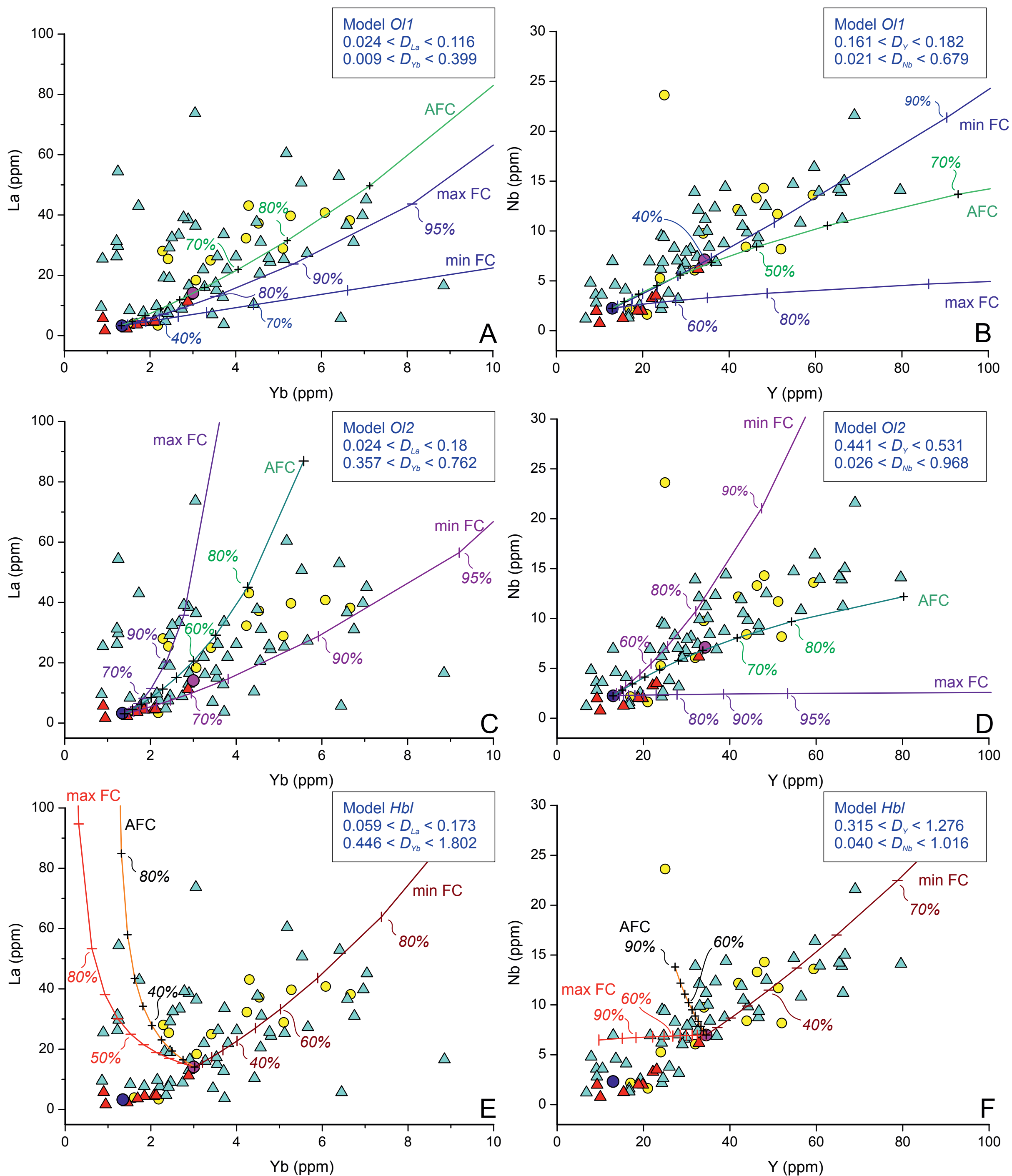


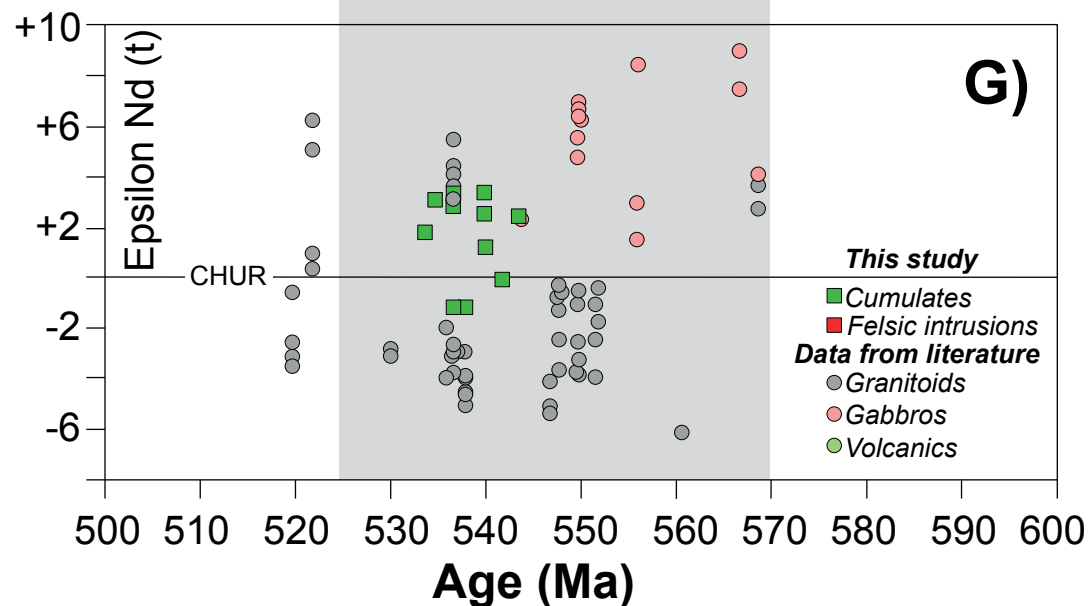
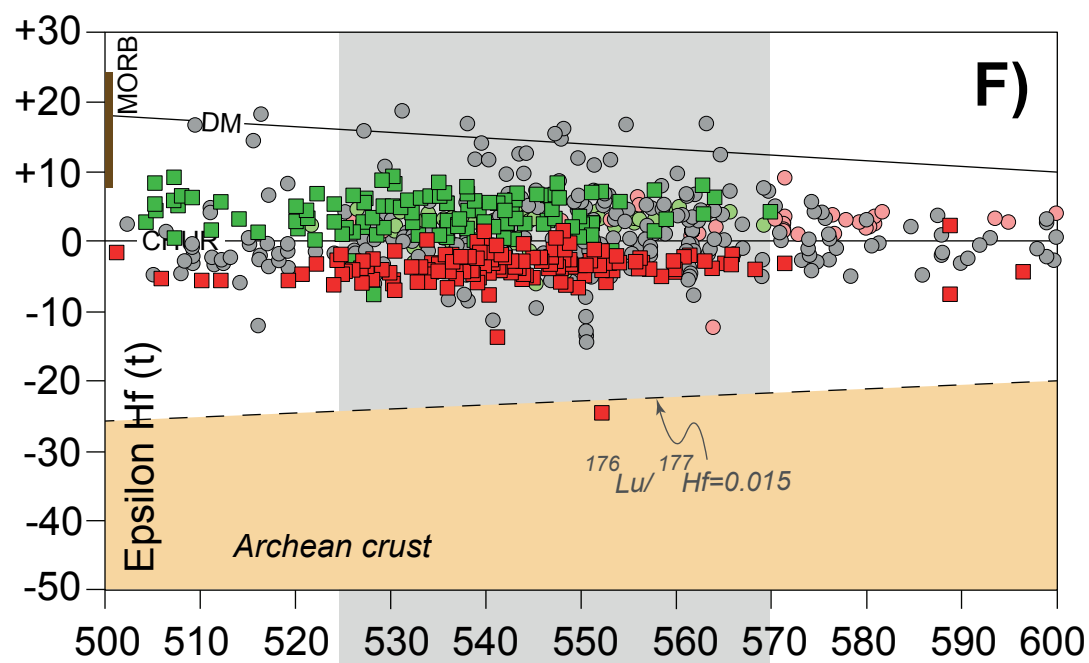
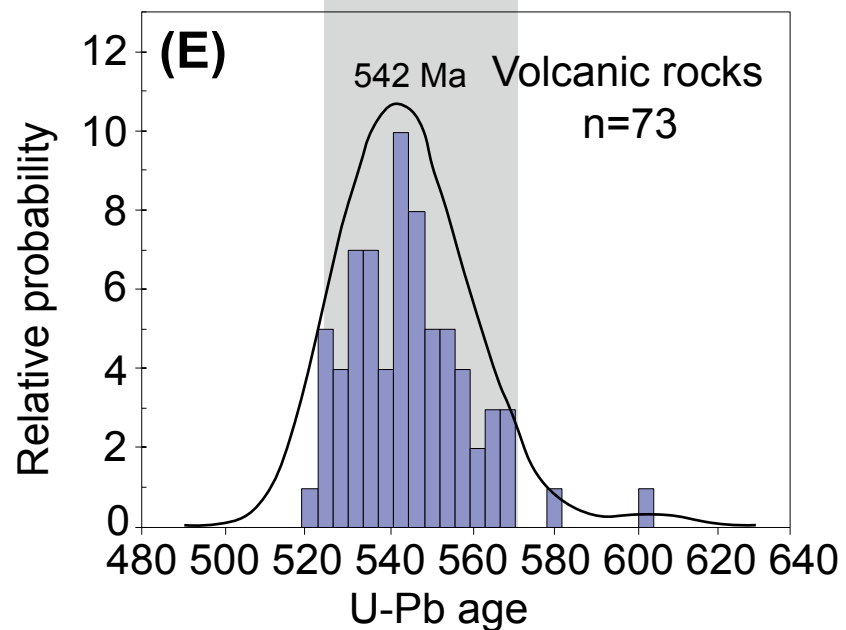
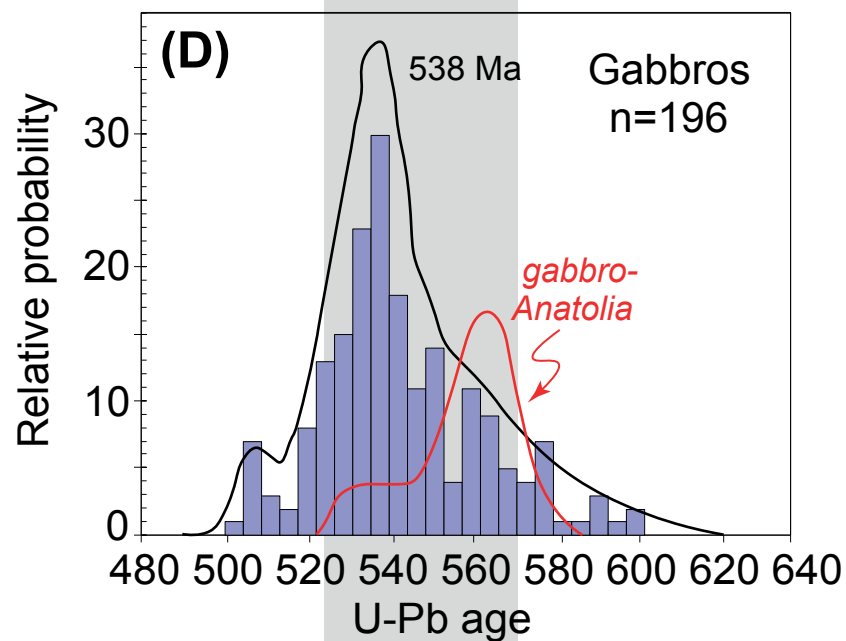
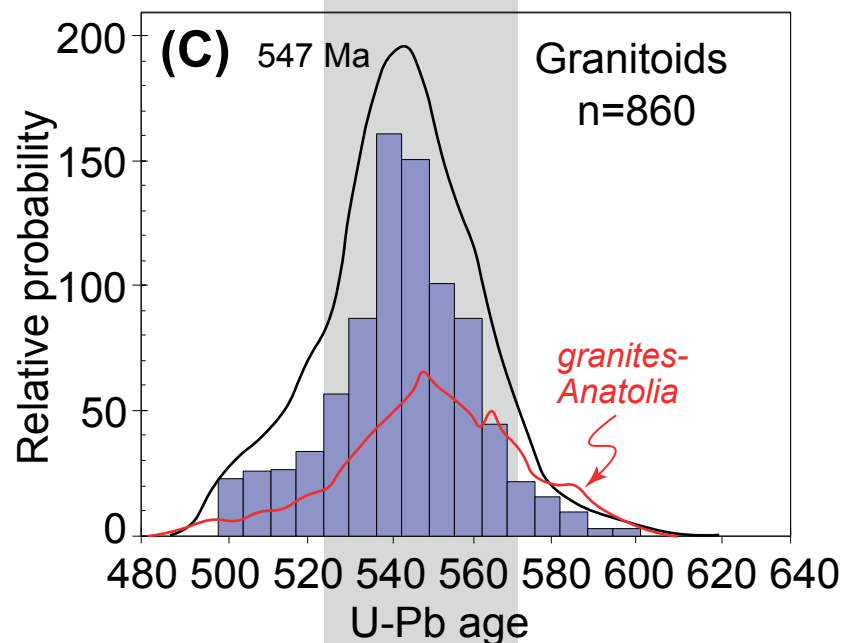
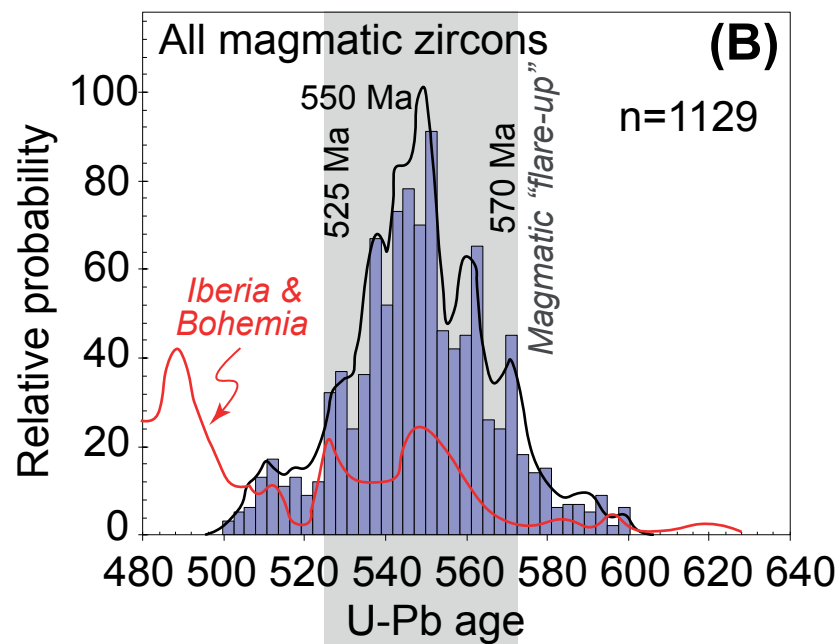
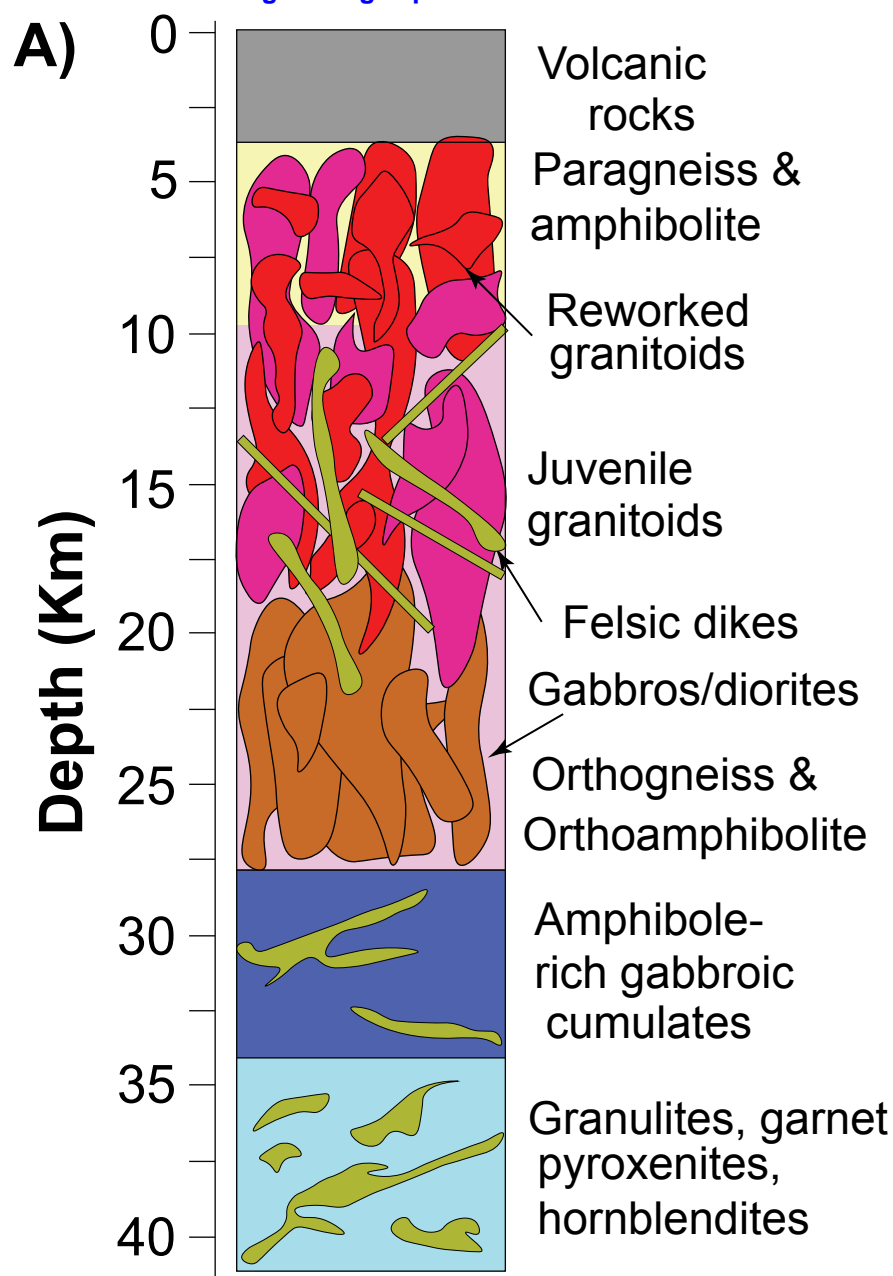












**Supplementary material for online publication only**

[Click here to download Supplementary material for online publication only: Appendix A.docx](#)

**Supplementary material for online publication only**

**[Click here to download Supplementary material for online publication only: Appendix B.docx](#)**

**Supplementary material for online publication only**

[Click here to download Supplementary material for online publication only: Fig. S1A.pdf](#)

**Supplementary material for online publication only**

[Click here to download Supplementary material for online publication only: Fig. S1B.pdf](#)

**Supplementary material for online publication only**

[Click here to download Supplementary material for online publication only: Fig. S1C.pdf](#)

**Supplementary material for online publication only**

[Click here to download Supplementary material for online publication only: Fig. S1D.pdf](#)

**Supplementary material for online publication only**

[Click here to download Supplementary material for online publication only: Fig. S1E.pdf](#)

**Supplementary material for online publication only**

[Click here to download Supplementary material for online publication only: Fig. S1F.pdf](#)

**Supplementary material for online publication only**

[Click here to download Supplementary material for online publication only: Fig. S2.pdf](#)

**Supplementary material for online publication only**

[Click here to download Supplementary material for online publication only: Fig. S3A.pdf](#)

**Supplementary material for online publication only**

[Click here to download Supplementary material for online publication only: Fig. S3B.pdf](#)

**Supplementary material for online publication only**

[Click here to download Supplementary material for online publication only: Table S1.xlsx](#)

**Supplementary material for online publication only**

[Click here to download Supplementary material for online publication only: Table S2.xlsx](#)

**Supplementary material for online publication only**

[Click here to download Supplementary material for online publication only: Table S3A.xlsx](#)

**Supplementary material for online publication only**

[Click here to download Supplementary material for online publication only: Table S3B.xlsx](#)

**Supplementary material for online publication only**

[Click here to download Supplementary material for online publication only: Table S4.xlsx](#)

**Supplementary material for online publication only**

[Click here to download Supplementary material for online publication only: Table S5.xlsx](#)

**Supplementary material for online publication only**

**[Click here to download Supplementary material for online publication only: Table S6A.xlsx](#)**

**Supplementary material for online publication only**

[Click here to download Supplementary material for online publication only: Table S6B.xls](#)

**Supplementary material for online publication only**

[Click here to download Supplementary material for online publication only: Table S7.xlsx](#)

**Supplementary material for online publication only**

[Click here to download Supplementary material for online publication only: Table S8.xlsx](#)

**Supplementary material for online publication only**

[Click here to download Supplementary material for online publication only: Table S9.xlsx](#)